Research Square

Preprints are preliminary reports that have not undergone peer review.
They should not be considered conclusive, used to inform clinical practice,
or referenced by the media as validated information.

Cholesterol Complexes of Redox-Active Nanoparticles Affect Redox Balance and Viability of Fibrosarcoma and Metastatic Bladder Cancer Cells

Nataliya Kavok
Institute for Scintillation Materials
Galyna Dudetskaya
Institute for Scintillation Materials
Vladyslav Seminko
seminko@ukr.net

Institute for Scintillation Materials
Pavel Maksimchuk
Institute for Scintillation Materials
Yurii Kot
V. N. Karazin Kharkiv National University
Olga Sedyh
Institute for Scintillation Materials
Vladimir Klochkov
Institute for Scintillation Materials
Svitlana Yefimova
Institute for Scintillation Materials

Research Article

Keywords: Nanoceria, Ascorbic acid, Complexes, Redox cycling, Antitumor activity

Posted Date: October 30th, 2026

DOI: https://doi.org/10.21203/rs.3.rs-11049033/v1

License: This work is licensed under a Creative Commons Attribution 4.0 International License.
Read Full License

Additional Declarations: No competing interests reported.

Cholesterol Complexes of Redox-Active Nanoparticles Affect Redox Balance and Viability of Fibrosarcoma and Metastatic Bladder Cancer Cells

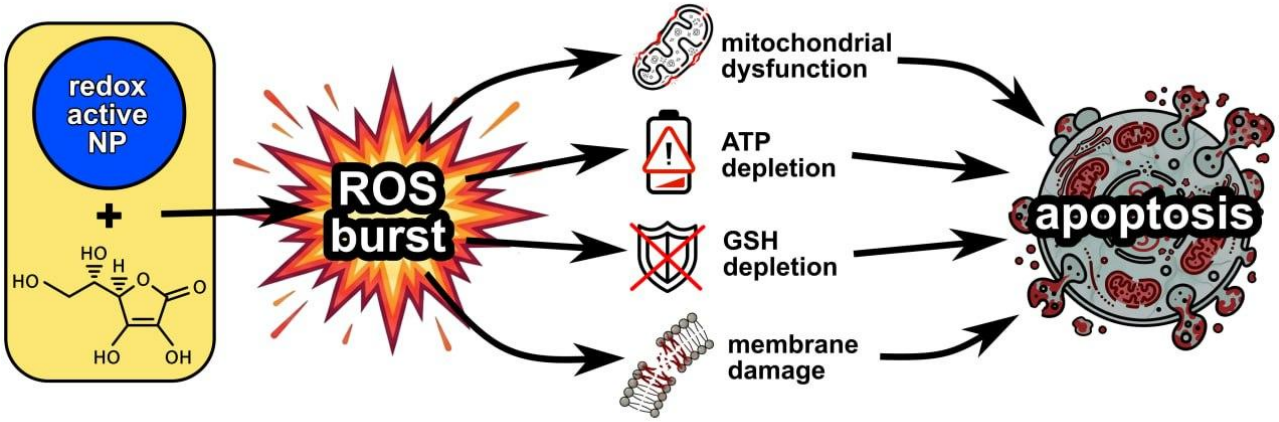
Nataliya Kavok[1] · Galyna Dudetskaya[1] · Vladyslav Seminko[1,2] * · Pavel Maksimchuk[1] · Yurii Kot[2] · Olga Sedyh[1] · Vladimir Klochkov[1] · Svitlana Yefimova[1]

* Corresponding Author: Vladyslav Seminko
e-mail: seminko@ukr.net

Abstract

Ascorbic acid (AA) is well-known for its concentration-dependent redox activity with anticancer effects at pharmacological (high) concentrations. However, its therapeutic efficacy varies significantly across cancer types highlighting the need for novel approaches. In this study, the ability of CeO_{2-x} and $GdYVO_4:Eu^{3+}$ NPs to provide redox imbalance and cell dysfunction as a result of enhanced ROS (reactive oxygen species) generation triggered by AA addition was revealed for fibrosarcoma (L929) and metastatic bladder cancer (T24T) cell lines. The observed potentiation of AA anticancer activity in combination with redox-active NPs is further enhanced in cholesterol-based supramolecular complexes (SMCs) incorporating NPs and menadione (vitamin K3), due to the synergistic action of their components. Comparison of several indicators of redox state of cancer cells (GSH/GSSG ratio, mitochondrial membrane potential, ATP, 8-isoprostane, and caspase-3 levels) revealed a higher antitumor efficacy of CeO_{2-x} NPs and CeO_{2-x}-based SMCs compared to $GdYVO_4:Eu^{3+}$ NPs that can be ascribed to their superior redox cycling capability and higher efficiency in ROS generation in combination with pharmacological ascorbate.

Graphical Abstract



Keywords Nanoceria · Ascorbic acid · Complexes · Redox cycling · Antitumor activity

Introduction

The ongoing search for new approaches to cancer treatment has recently led to an idea to use specific properties of tumor microenvironment (low pH, high ROS level) for enhanced anticancer therapy. One of specific features of cancer cells is the high activity of antioxidant defense systems due to an excessive amount of ROS produced inside these cells [1]. Redox-adaptive mechanisms in tumor cells include an activation of redox-sensitive transcription factors (such as NF-κB and Nrf2) [2], increased level of ROS-scavenging molecules (such as glutathione) [3], and genetic or epigenetic alterations affecting redox regulation [4]. Consequently, a promising therapeutic strategy involves further increase of ROS concentration using external ROS-generating agents (for instance, ROS-generating nanoparticles [5]) in order to overcome the limits of ROS-defending system of tumor cells. Under conditions of disrupted redox homeostasis and persistent oxidative stress, the ROS burst induced by such nanoparticles can shift tumor cells from the state of up-to-the-edge equilibrium toward irreversible death [6].

Besides ROS-generating nanoparticles, the strong anticancer effect was reported for high concentrations of ascorbic acid (AA) [7]. The mechanism of anticancer activity of AA is related to an effect of H_2O_2 formed at AA autoxidation on the ROS-dependent mitochondrial pathways in tumor cells [8]. At the same time, the practical use of AA in cancer therapy is limited due to requirement of extremely high doses which are not achievable under physiological conditions [9]. The anticancer effect of AA enhances sufficiently in the presence of redox cycling agents such as menadione (vitamin K3) allowing decreasing the required AA concentrations to pharmacologically achievable values [10, 11]. The combination of AA and menadione taken in 100:1 ratio (Apatone® trademark) in 2008 has successfully passed the phase I/IIa clinical studied for the treatment of prostate cancer patients who have failed standard therapy [12]. Later studies have shown that in endometrioid ovarian carcinoma (MDAH 2774) cells the combination of AA and vitamin K3 caused cell death by the mechanism of autoschizis, a type of cell death which does not require caspase-3 activation, and so allows to bypass the complex defense systems of cancer cells that make them resistant to traditional chemotherapy [13]. An additional advantage of these approach over standard methods of cancer treatment is a rather low systemic toxicity of both AA and vitamin K3 minimizing adverse effects in non-cancer cells. The results obtained for the combination of AA and menadione launched a series of studies on other combinations of AA (or other molecules with high reducibility) with redox cycling agents of different types [14].

The sufficient advances in this field can be expected for AA combinations with so-called nanozymes, i.e. NPs, which can mimic the activity of various enzymes (first of all, of oxidoreductase family) due to presence of ions with variable valence (Ce^{3+}/Ce^{4+}, Fe^{2+}/Fe^{3+}, Mn^{3+}/Mn^{4+} etc) [15]. Potential for combining Fenton-like activity of Fe^{2+}/Fe^{3+} redox pair with generation of H_2O_2 at AA autoxidation and high reducing ability of AA was demonstrated for a number of iron-containing NPs such as Fe_3O_4 [16], Fe_3O_4@C [17], FeOCl@H-DMOS [18], and $Fe_{1-x}O$ [19] NPs. In addition to Fe-containing NPs, combinations of AA with nanozymes based on other transition metals, such as copper (Cu) [20], manganese (Mn) [21], cobalt (Co) [22], and palladium (Pd) [23] were studied. Generally, it can be concluded that NPs with

oxidoreductase activity can function as redox mediators and catalysts facilitating electron transfer processes between AA and biomolecules [14].

Prooxidant activity for nanoceria (CeO_{2-x}) and vanadium-based nanoparticles at pH values typical for cancer cells was reported in a number of publications [24, 25]. High oxidative ability (including direct oxidation of a number of thiol-containing molecules [26, 27]) and efficient ROS generation by these NPs at acidic pH values allows to consider these NPs as perspective antitumor agents. The reversible $Ce^{3+}\leftrightarrow Ce^{4+}$ and $V^{4+}\leftrightarrow V^{5+}$ redox cycling is a key mechanism allowing these NPs to affect intracellular ROS levels in both normal and cancer cells (down- and up-regulation, respectively) [28]. The effect of ROS generation can be enhanced in the presence of reducing agents such as AA enabling effective electron donation to NPs. This process generates ascorbyl radicals and dehydroascorbic acid, key intermediates that are crucial for AA-mediated anticancer activity.

Cancer cells are cholesterol-dependent and an uptake of extracellular cholesterol is often elevated in cancer cell to meet its metabolic needs [29]. To enhance affinity for the target cell membranes $GdYVO_4:Eu^{3+}$ NPs-based cholesterol complexes were developed and successfully applied earlier in treatment cancer cells to inhibit the tumor growth and to increase the survival [30]. At the same time, an increase of anticancer effect of cholesterol complexes of CeO_{2-x} and $GdYVO_4:Eu^{3+}$ NPs can be expected in the presence of AA.

In our previous paper [31] we demonstrated that nanoceria-based supramolecular complexes (SMC) with menadione and cholesterol exhibit pronounced ascorbate-triggered antitumor activity in both 2D and 3D models of the mouse fibrosarcoma L929 cells. However, the studies were limited by one type of cancer cells (L929 fibrosarcoma cells), and one type of redox-active NPs (CeO_{2-x}). In this paper we show the applicability of the same approach of triggering cell apoptosis for SMC based on different types of redox-active NPs (CeO_{2-x} and $GdYVO_4:Eu^{3+}$), and for different cell lines (besides mouse fibrosarcoma L929 cells, T24T cells, a highly metastatic derivative of the human bladder cancer T24 cell line was used). T24T cell line is a classical, widely accepted model of metastatic (secondary) cancer for high-throughput *in vitro* screening of antitumor compounds [32]. The choice of T24T cells was additionally supported by enhanced GLUT1 activity in this cell line [33] stimulating intracellular uptake of oxidized ascorbate species (DHA), which are reduced back to AA inside the cell at the expense of glutathione (GSH) and NADPH. Previous studies have shown that the combination of AA and menadione triggers cell death in T24T cell line by the mechanism of autoschizis [34]. The results obtained in our paper clearly confirm the generality of the approach for cancer treatment using the effect of AA-triggered ROS generation by redox cycling agents including NPs and NPs-based SMCs with menadione and cholesterol. At the same time, direct comparison of anticancer activity of nanoceria and $GdYVO_4:Eu^{3+}$ NPs revealed sufficiently less efficiency of the second ones that can be ascribed to different redox and ROS-generating properties of these NPs. The observed differences in the underlying mechanisms are attributed to the enhanced pH-dependent ROS generation (boosting) achieved when ascorbic acid (AA) is combined with CeO_{2-x} nanoparticles and their complexes. The observed differences are mechanistically driven by the strong pH-dependent potentiation of ROS generation as well as AA-derived oxidative

intermediates formed upon combination of ascorbic acid (AA) with CeO_{2-x} nanoparticles and their complexes.

Materials and methods

Obtaining of Nanoparticles and NPs-based SMC

Colloidal aqueous dispersions of NPs were prepared via a hydrolysis-based colloidal synthesis starting from lanthanide (III) chlorides. The reagents used in the synthesis included cerium chloride heptahydrate ($CeCl_3 \cdot 7H_2O$, 99.9%, Acros Organics), yttrium chloride heptahydrate ($YCl_3 \cdot 7H_2O$, 99.9%, Acros Organics), gadolinium chloride heptahydrate ($GdCl_3 \cdot 7H_2O$, 99.9%, Acros Organics), europium chloride heptahydrate ($EuCl_3 \cdot 7H_2O$, 99.9%, Acros Organics), anhydrous calcium chloride ($CaCl_2$, 93%, Sigma-Aldrich), sodium citrate ($Na_3C_6H_5O_7$, 99.0%, Macrokhim), ammonium hydroxide (NH_4OH, 25 wt%, Sigma-Aldrich), anhydrous sodium metavanadate ($NaVO_3$, 96%), and HMTA (99.0%, Macrokhim).

Nanoceria was obtained according to the following procedure. An aqueous $CeCl_3$ solution (200 ml, 0.008 mM) was combined with 200 ml of sodium citrate solution (0.008 M), followed by the addition of 400 ml of HMTA solution (0.08 M). The mixture was stirred for 3 h at ambient temperature. Subsequently, 0.7 ml of NH_4OH and 1.4 ml of H_2O_2 were added. The resulting solution was transferred to a round-bottom flask and heated under reflux for 5 h. After reflux, a 1 M $CaCl_2$ solution was added dropwise until turbidity appeared, indicating particle formation. The precipitated solid was isolated by centrifugation and repeatedly washed with distilled water. In the final step, an aqueous sodium citrate solution was added to achieve NPs:$Na_3C_6H_5O_7$ molar ratio of 1:1.

The aqueous colloidal solutions of $Gd_{0.7}Y_{0.2}Eu_{0.1}VO_4$ (OV) NPs were synthesized according to the following method. 10 ml of aqueous solutions of 0.01 M lanthanide chlorides (7 ml of $GdCl_3$, 2 ml of YCl_3, and 1 ml of $EuCl_3$) was mixed with 8 ml of sodium citrate solution (0.01 M). Then, 8 ml Na_3VO_4 (0.01 M) obtained by adding NaOH (1 M) to $NaVO_3$ was added dropwise (pH = 13) into the obtained solution. The mixture was intensively stirred using a magnetic stirrer until a yellowish transparent solution was formed. The solution was heated on a water bath for 30 min for 24 h at 100 °C. Then, the obtained colorless transparent solution was cooled and dialyzed with a molecular weight cut-off of 12 kDa against water for 24 h to remove the excess of ions.

NPs-based SMC were obtained in the following way. Acetone solution of menadione (1 g/l) was mixed with 2 ml of complexes of NPs and cholesterol containing nanoceria or OV NPs (1 g/l) and cholesterol (0.02 g/l). Then 20 ml of distilled water was added to the solution and stirred again for 10 minutes. The resulting solution was transferred to a round-bottom flask and concentrated to a final volume of 5 ml using a rotary evaporator at 50 °C. This procedure yielded transparent, weakly opalescent aqueous dispersions containing NPs at a concentration of 1 g/l, cholesterol at 0.02 g/l, and menadione at 0.4 g/l. The dispersions remained stable when stored in the dark for at least two weeks, with no observable changes in their properties.

Characterization of Nanoparticles and NPs-based SMC

The sizes of obtained NPs were determined using high-resolution transmission electron microscopy (JEOL JEM-2100F (with Schottky-type field emission gun) and JEOL JEM-2100 (with LaB6 filament)). High-resolution TEM images were analyzed using Gatan DigitalMicrograph v3.3 Software to obtain the interplane distances from the crystalline structure of individual nanoparticles. The hydrodynamic diameters of NPs and SMC in colloidal solutions were determined using the methods of dynamic light scattering (DLS) with a ZetaPALS/BI-MAS analyzer (Brookhaven Instruments Corp., USA).

X-ray diffraction methods (Bruker D8 Discover powder diffractometer, Cu Kα radiation) were used to determine the structure of NPs. Phase identification was performed using PDF-4+ 2023 International Center for Diffraction Data ICDD-database. Crystal size was analyzed by Rietveld refinement using HighScore Plus Crystallographic Software and Si standard.

X-ray photoelectron spectroscopy (XPS) was used to find the valence state of cerium and vanadium ions in obtained NPs. The XPS experiments were performed on a film of NPs obtained after drying the NPs colloidal solutions on the gold foil. The measurements were carried out with a Physical Electronics PHI 5600 spectrometer, featuring a 150 mm hemispherical analyzer and a monochromatic Al Kα X-ray source (200 W). High-resolution spectra were recorded with a pass energy of 29.35 eV and a spot size of 0.8 mm. To prevent surface alteration during analysis, a low-energy electron gun set to 5 V was employed as a neutralizer. All spectra were energy-calibrated using adventitious carbon at 284.8 eV as a reference point.

DSC measurements were performed using a Mettler DSC 1 microcalorimeter (Mettler-Toledo). A sample was placed into a 40 μL aluminum crucible hermetically sealed with a lid. DSC profiles were obtained in heating regime (25 °C to 170 °C) at the 10 °C/min scanning rate. Processing of the original data were performed by means of Star^{e} 11.0 software. Sample weights of pure components were taken the same as in SMC.

Oxidation of Ascorbic Acid by CeO_{2-x} and OV Nanoparticles and NPs-based SMC

The oxidation of ascorbic acid was monitored by spectroscopic techniques. The solutions of studied NPs (with final concentrations of 10, 20, and 40 μg/ml) were added to 10 mM HEPES buffer (pH 6.7 - 7.8) contained 200 μM of ascorbic acid. The mixture was kept for 60 min at 37 °C. The changes in ascorbic acid level were quantified by measuring its absorbance at λ_{max} = 265 nm using Specord 200 spectrophotometer (Analytik Jena, Germany). The ascorbic acid solution without NPs was used as control. The loss of ascorbic acid was expressed as relative change (as a reference the absorbance at 0 h was used).

Cell Culture

L929 mouse fibrosarcoma cells and T24T human bladder carcinoma cells were provided by a IPCC NASU and Karazin NU collections cell cultures (Kharkiv,

Ukraine). Cells were cryopreserved in the culture medium containing 10% DMSO (v/v) and stored in liquid nitrogen. Cryopreservation of cells was carried out using cooling rate of 1°C/min in automatic controlled rate freezer Asymptote EF600M (Grant Instruments) to −40°C, and then cryovials were plunged into cryogenic liquid nitrogen system Biorack 3000 (Statebourne). Thawing of the samples was performed in water bath MyBath 4L (Benchmark Scientific) at 40 °C. Cryoprotectant was removed by gradual addition of DMEM/F12 medium to 1 ml of sample until the total volume was 10 ml. After dilution of cryoprotective medium the cells were centrifuged 3 min at 325 x g using Durafuge 300 (Thermo Scientific), the supernatant was removed and the cells were used for cultivation.

After freezing / thawing procedure cell viability was (95.8±6.5) % as determined by trypan blue dye-exclusion test using 0.4% trypan blue solution (Gibco) and automated cell counter Countess (Invitrogen).

Cells were seeded at an average density of $2.5x10^4$ cells/ml into 175 cm^2 culture flask (1 million cells in 40 ml of medium). L929 cells were cultured in DMEM/F12 medium supplemented with 10% fetal bovine serum, 200 U/ml penicillin, 400 µg /ml streptomycin and 5 µg /ml amphotericin B in a humidified atmosphere at 37°C and 5% CO_2 using Galaxy 14S incubator (Eppendorf). T24T cells were grown as a monolayer in complete RPMI (RPMI-1640 medium supplemented with 10% fetal calf serum, 100 U/mL penicillin and l00 µg/mL streptomycin), in a humidified atmosphere with 7% CO_2 at 37°C using Galaxy 14S incubator (Eppendorf). Under these conditions, the plating efficiency was 80–90% and the doubling time was 9–10 h. Single cell suspensions were obtained by trypsinization of monolayer cultures.

The culture medium was changed every 3-4 day. After the monolayer was formed, the cells were subcultured as advised by ATCC organization: 0,25% Trypsin-EDTA solution was added to flask until cell layer is dispersed (about 5-10 min). After that growth medium was added and cells were aspirated by gently pipetting. Aliquots of cell suspension were added to 12 well culture plates (Corning, USA) at a density of $0.3\text{-}1.0x10^5$ cells/ml. A subcultivation ratio was 1:10. Cells were cultured under the conditions described above for 1 day, after which nanoparticles were added.

Confocal Microscopy

The imaging of the caspases 3 in live T24T and L929 cells was carried out by confocal microscopy at excitation 535 nm/emission 620 nm using the Caspase Multiplex Activity Assay Fluorometric Kit (Abcam, ab219915) in accordance with the manufacturer's instructions. Just before imaging, the growth medium with nanoparticles was removed and replaced with prewarmed using "Live-cell imaging solution" (Life Technologies). The imaging of the NPs-based SMCs directly in live cells was carried out by confocal microscopy at excitation 391 nm/emission 618 nm (OV NPs-based SMC) and excitation 350 nm/emission 423 nm (CeO_{2-x}-based SMC) as described below. The nucleus is counterstained with fluorogenic, DNA-selective and cell-permeant dye Nuclear Green LCS1 (Abcam, ab138904) and visualized at excitation 473 nm/emission 532 nm.

Cell visualization was performed on a laser scanning confocal microscope FV10i-LIV (Olympus, Japan) equipped with a 60/1.2 NA water immersion objective

and a system of intravital cell incubation (37.0 ± 0.1°C, 5.0 ± 0.1%CO_2, 99.5 ± 0.1% RH). Cells monolayers were visualized directly in 35 mm confocal dish (VWR, 75856-742). Confocal images were acquired with a scanning mode format of 1024×1024 pixels. The pinhole aperture was 1 Airy unit. Confocal images shown are representative images of 10 fields of view. The 3D imaging dataset is assembled from 50 optical sections in the regions of interest. Post-rendering of the obtained images including cells autofluorescence subtraction was performed using Olympus cellSence software (Olympus licensed).

Cells Viability Assay

Cells viability was assayed directly in live cells by "Calcein AM Assay Kit (Fluorometric)" (Abcam, ab228556) according to the manufacturer's recommendations. Calcein AM is a non-fluorescent, hydrophobic compound that easily penetrates intact and live cells. During the Calcein AM assay, hydrolysis of Calcein AM by intracellular esterases produces a hydrophilic, strongly fluorescent compound that is retained in the cell cytoplasm and can be measured at Ex/Em = 485/530 nm. The measured fluorescence intensity is proportional to the number of viable cells. Briefly, the Calcein AM Cell Dye reagent was added to 0.25 mL of pre-warmed (37^0C) Assay Buffer and after vortexing (IKA TTS3 shaker, 4 sec) the solution was immediately added to the cell's monolayer. Before monitoring, the cells were incubated with the dye for 30 min at 37^0C in the dark using Galaxy 14S incubator (Eppendorf). The assay of fluorescence intensity in cells was carried out on a FL600 microplate multimodal reader (BioTek) at excitation of 485 nm/emission 530 nm and calculated as RFU/10^3 cells.

ROS Assay

Intracellular reactive oxygen species (ROS) levels were quantified in L929 and T24T cells using the *DCFDA Cellular ROS Detection Assay Kit* (Abcam, ab113851) following the manufacturer's protocol. This assay employs the cell-permeable probe 2′,7′-dichlorofluorescein diacetate (DCFDA), which detects hydroxyl and peroxyl radicals as well as other ROS. After entering the cell, DCFDA is deacetylated by intracellular esterases to a nonfluorescent intermediate that is subsequently oxidized by ROS to the green-fluorescent product 2′,7′-dichlorofluorescein (DCF).

Prior to fluorescence measurements, cells grown as monolayers were pretreated with nanoparticles (NPs) or supramolecular complexes (SMCs) for 24 h. A 20 mM DCFDA stock solution was diluted in pre-warmed (37 °C) phenol-red-free DMEM supplemented with 10% FBS to a final concentration of 25 μM and added to each well of a 12-well plate. Cells were incubated with the probe for 45 min at 37 °C in the dark using a Galaxy 14S incubator (Eppendorf). ROS-dependent fluorescence was recorded at excitation/emission wavelengths of 485/535 nm using an FL600 multimode microplate reader (BioTek). Measurements were performed after 24, 48, and 72 h of cultivation.

Superoxide and Hydroxyl Radical Assay

Superoxide and hydroxyl radical production in live cells was assessed by fluorometric analysis using dihydroethidium (DHE) as a superoxide-sensitive probe and aminophenyl fluorescein (APF) as a hydroxyl radical-specific indicator. Oxidation of DHE by superoxide results in the formation of 2-hydroxyethidium (Ex/Em = 530/620 nm), whereas APF is converted to highly fluorescent fluorescein upon reaction with hydroxyl radicals (Ex/Em = 490/515 nm). Fluorescence measurements were carried out using an FL600 multimode microplate reader (BioTek).

Cell Lysate Preparation

Cells were homogenized in cooled at 4°C Tris buffer (50 mM tris-HCl, 150 mM NaCl, pH 7.5) and centrifuged at 4°C and 13000g for 5 min by Biofuge Fresco centrifuge (Thermo Scientific). Then, a supernatant was collected in a Biocision CoolRack (4.0°C) and used to determine 8-isoprostane and reduced and oxidized glutathione states. Determination of total protein in cell lysate was carried out by the direct UV spectrophotometric method on a scanning spectrophotometer Ultrospec 3100 pro (Amersham Biosciences).

GSH/GSSG Assay

The intracellular levels of reduced (GSH) and oxidized (GSSG) glutathione in cell lysates were quantified by fluorometric analysis using the *GSH/GSSG Ratio Detection Assay Kit (Fluorometric–Green)* (Abcam, ab138881). Fluorescence measurements were obtained with an FL600 multimode microplate reader (BioTek) at excitation/emission wavelengths of 490/520 nm following a 30 min incubation. The redox status was expressed as the ratio of GSH to GSSG. Under physiological conditions, the majority of cellular glutathione (>90%) exists in the reduced form, whereas oxidative stress leads to GSSG accumulation and a concomitant decrease in the GSH/GSSG ratio.

8-isoprostane Assay

Determination of the content of 8-isoprostane in the cell lysate was performed by ELISA method with spectrophotometric detection (450 nm) on a FL600 microplate multimodal reader (BioTek) using test kits "8 isoprostane ELISA Kit" (Abcam, ab175819). The content of parameter was calculated in fg/μg of protein.

ATP Assay

Intracellular ATP levels in L929 and T24T cells were determined using a luminescence-based method with the *Luminescent ATP Detection Assay Kit* (Abcam, ab113849). Measurements were performed on an FL600 multimode microplate reader (BioTek). The assay relies on light emission generated by the luciferase–luciferin reaction in the presence of ATP, with the resulting luminescence directly

proportional to cellular ATP content. ATP concentrations were calculated from a calibration curve and expressed in micromolar units (μM).

Mitochondrial Membrane Potential Assay

The mitochondrial membrane potential ($\Delta\psi_m$) in L929 and T24T cells was assessed by fluorescence measurements using a ratiometric JC-1 probe (Abcam, ab113850) and a FL600 multimode microplate reader (BioTek). Changes in $\Delta\psi_m$ were quantified as the ratio of fluorescence intensities corresponding to JC-1 aggregates (Ex/Em = 460/590 nm) and monomeric forms of the dye (Ex/Em = 460/530 nm). Under conditions of reduced $\Delta\psi_m$, JC-1 is present primarily in its monomeric form and emits green fluorescence, whereas elevated $\Delta\psi_m$ promotes probe aggregation accompanied by orange fluorescence. Accordingly, a reduction in aggregate-associated fluorescence reflects mitochondrial depolarization, while an increase indicates hyperpolarization.

Caspase-3 Assay

Caspase-3 activity in live cells was measured using the *Caspase Multiplex Activity Assay Fluorometric Kit* (Abcam, ab219915) in accordance with the manufacturer's instructions. The assay is based on the fluorogenic substrate DEVD-ProRed, which releases the red-emitting ProRed™ fluorophore upon cleavage by active caspase-3. For the assay, the DEVD-ProRed reagent was diluted in 0.5 ml of pre-warmed assay buffer (37 °C), briefly vortexed (IKA TTS3 shaker, 4 s), and immediately applied to the cell monolayer to achieve a final probe concentration of 0.1 μM. Cells were then incubated with the dye for 30 min at 37 °C in the dark using a Galaxy 14S incubator (Eppendorf). Fluorescence was subsequently recorded using an FL600 multimode microplate reader (BioTek) at an excitation wavelength of 535 nm and an emission wavelength of 620 nm. Caspase-3 activity was expressed as relative fluorescence units normalized to 10^3 cells (RFU/10^3 cells).

Statistical Analyses

Deviations were analysed by Shapiro-Wilk test. Subsequent analysis included one-way ANOVA with Dunn-Sidak post-hoc test or Kruskal-Wallis ANOVA with Mann-Whitney post-hoc test. The values were expressed as mean ± SEM from 3 to 12 independent experiments performed in duplicate, and the results were considered statistically significant at $p < 0.05$.

Results

Characterization of Nanoparticles and NPs-based SMC

The obtained NPs were characterized using TEM, XRD, and XPS methods (Fig. 1).

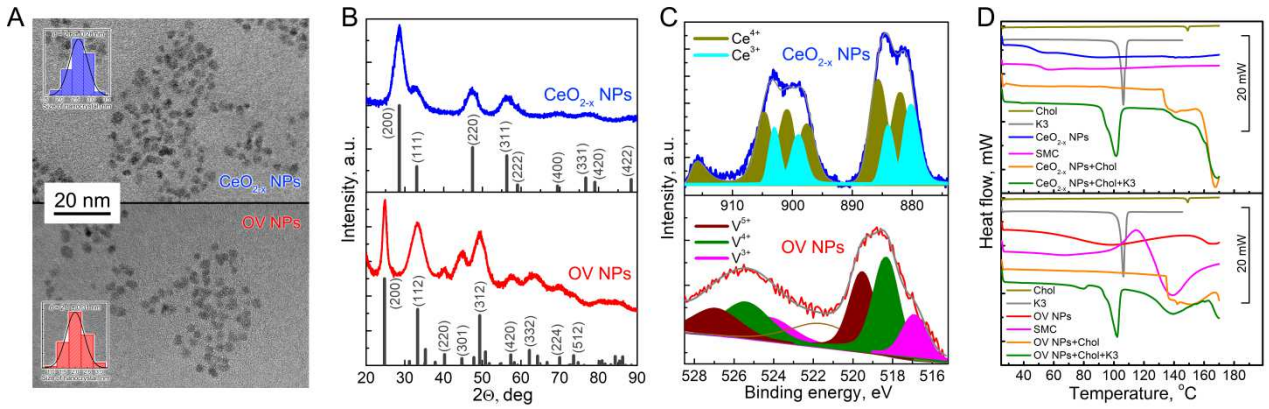


Fig. 1 A) TEM images of CeO_{2-x} and $GdYVO_4:Eu^{3+}$ (OV) NPs with size distributions in the insets; B) XRD of CeO_{2-x} and $GdYVO_4:Eu^{3+}$ NPs; C) XPS of CeO_{2-x} and $GdYVO_4:Eu^{3+}$ NPs; D) DSC of supramolecular complexes of CeO_{2-x} and $GdYVO_4:Eu^{3+}$ NPs.

The analysis of TEM images indicates that the average sizes of CeO_{2-x} NPs are 2.6 ± 0.28 nm, and that of OV NPs are 2.1 ± 0.31 nm (Fig. 1A). The sizes of both NPs are close enough to enable direct comparison of prooxidant properties of these NPs. XRD of nanoceria and OV NPs are shown in the Fig. 1B. According to XRD, CeO_{2-x} NPs preserve fluorite-type structure typical for bulk ceria (JCPDS card No.34-0394), while OV NPs have tetragonal zircon-type structure (JCPDS card No.72-0277). The sizes of crystallites determined from XRD agree well with the sizes of NPs revealed by TEM (~2.4 nm). XPS studies (Fig. 1C) reveal that even without reducing agent (such as AA), nanoceria and OV NPs contain high amounts of Ce^{3+} (32%), and V^{4+} (45%)/V^{3+} (17%) ions, respectively. Coexistence of ions with different valence states in both NPs determines their ability to take part in redox reactions (including ROS generation).

In order to improve biocompatibility and improve ROS generation properties, the cholesterol-based supramolecular complexes (SMC) of nanoceria and OV NPs with menadione were obtained. The formation of SMC on the base of both types of NPs was confirmed using dynamic light scattering (DLS) and differential scanning calorimetry (DSC) methods. The DLS data for both nanoceria and OV NPs-based SMC indicate a sufficient increase of the size compared to colloidal solutions of NPs. The hydrodynamic diameters of CeO_{2-x} NPs and OV NPs were 8.3±0.3 nm and 25.0±1.3 nm, respectively, while for SMC the hydrodynamic diameters increased to 171.2 ± 1.7 nm (with polydispersity index (PI) of 0.27) for nanoceria, and to 131.7 ± 6.1 nm (with PI of 0.347) for OV NPs.

Complexation of all SMC components for nanoceria-based and OV-based SMC was supported by DSC results (Fig. 1D). In the Fig. 1D the thermograms of the SMC, separate components of SMC, and mechanical mixture of SMC components

are shown. The thermogram of pure cholesterol contains the endothermic melting peak with temperature of 149 °C and enthalpy of ~28 kJ/mol. Pure menadione is characterized by the endothermic peak with temperature of 107 °C and enthalpy of 20±1.2 kJ/mol related to its melting. In mechanical mixture of SMC components for both types of SMC this peak is also observed, with slight broadening and shift towards lower temperatures. However, the characteristic peaks of both menadione and cholesterol are absent in thermograms of both nanoceria-based and OV-based SMC indicating their entire inclusion into SMC structure.

Uptake and Intracellular Distribution of NPs-Based SMC in L929 and T24T Cancer Cells

Enhanced uptake of cholesterol-based complexes of OV NPs by cancer cells (including Ehrlich carcinoma and HepG2) was observed in our previous studies [30]. The same effect was revealed for L929 and T24T cell lines for SMC based on both CeO_{2-x} and OV NPs. At the same time the intracellular distribution of CeO_{2-x} and OV NPs follows the different patterns (Fig. 2), and while OV NPs are accumulated within cell nuclei (that can be seen from comparison of 3D reconstruction results with and without subtraction of fluorescence of Nuclear Green LCS1 dye), CeO_{2-x} NPs are mainly located within cell cytoplasma. Nuclear localization of OV NPs is potentially more favourable for anticancer activity as it allows ROS generated by these NPs to interact directly with DNA, chromatin, or nuclear proteins increasing the probability of oxidative damage to these critical cellular targets, which could enhance the cytotoxicity of NPs and NPs-based SMC.

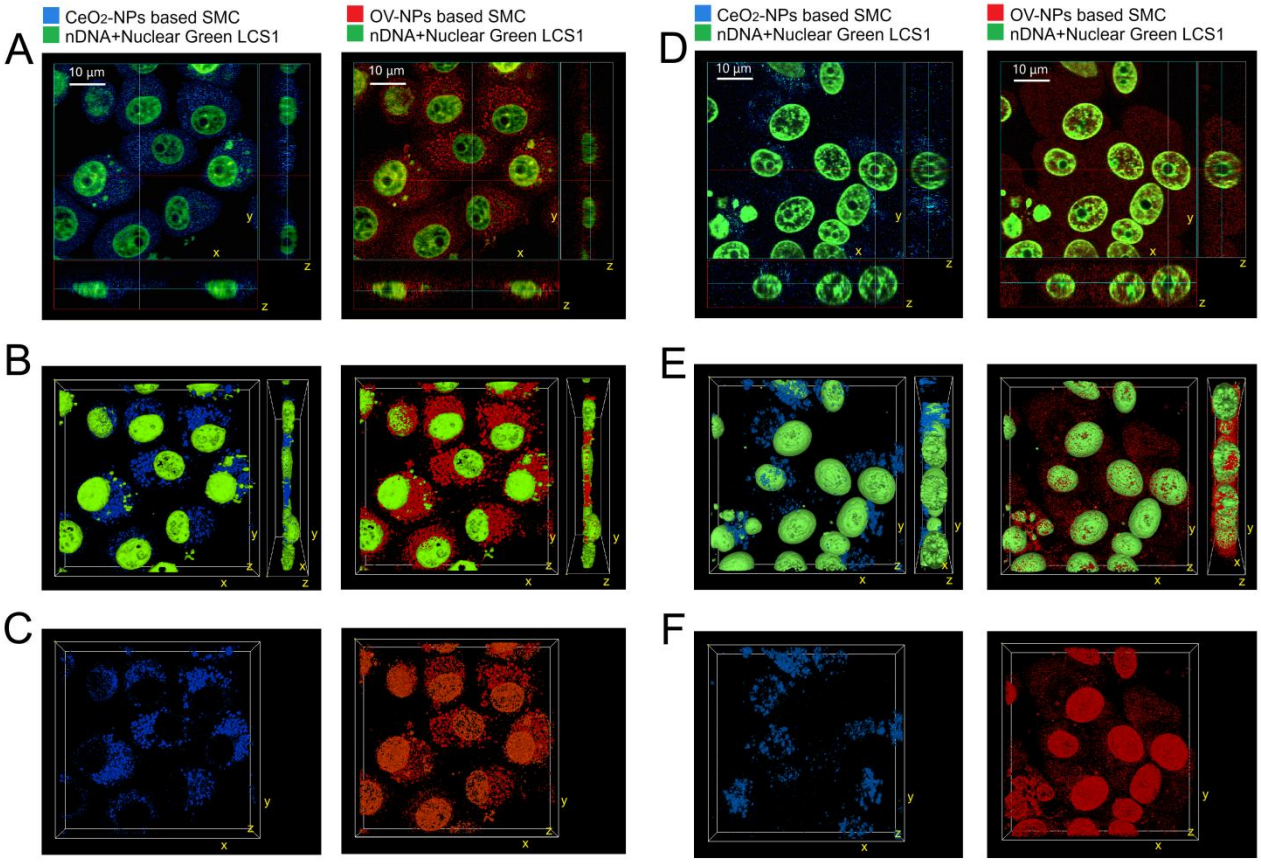


Fig. 2 Intracellular distribution of CeO_{2-x} and $GdYVO_4:Eu^{3+}$ (OV) NPs after uptake of NPs-based SMC by L929 (A-C) and T24T (D-F) cells: A, D – confocal images, B, E – 3D reconstruction, C, F - 3D reconstruction with green fluorescence subtraction.

Oxidation of Ascorbic acid by Nanoceria and OV NPs

In our previous studies, ascorbic acid (AA) was proposed as an electron donor triggering ROS generation via redox cycling of nanoparticles (NPs) [27, 31]. According to this concept, the AA–NP pair acts similarly to the well-known AA–menadione system, with electron transfer occurring first from AA to the NP (AA oxidation), followed by transfer from the NP to molecular oxygen, resulting in superoxide formation ($O_2 + e^- \rightarrow O_2^{\bullet-}$) and its subsequent conversion into other ROS. The applicability of this mechanism was experimentally confirmed using CeO_{2-x} and $GdYVO_4:Eu^{3+}$ (OV) of comparable size (~2 nm). The former are known for their efficient redox cycling ($Ce^{3+} \leftrightarrow Ce^{4+}$) determining their self-regenerable redox properties during nanoceria-ROS interaction [35], while for the latter the redox cycling ($V^{4+} \leftrightarrow V^{5+}$) is less efficient and more limited under physiological conditions [36]. The oxidation of ascorbic acid by nanoceria and OV NPs was determined from the change of characteristic AA absorption band with λ_{max} = 265 nm at different pH values in the presence of different concentrations of NPs (Fig. 3).

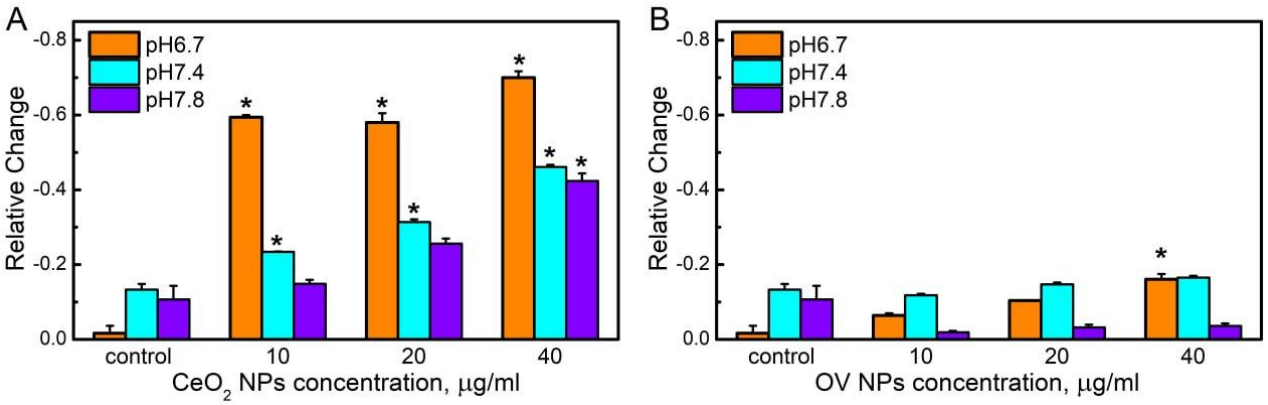


Fig. 3 Oxidation of ascorbic acid (C = 200 μM, t = 1 h, 37 °C) by CeO_{2-x} **(A)** and $GdYVO_4:Eu^{3+}$ (OV) nanoparticles **(B)** at different pH values (6.7, 7.4, and 7.8), and different concentrations of NPs. * $p<0.05$ – compared to control, ascorbic acid absorbance at 0 min –3.248±0.028 a.u.

For both types of NPs, concentration increase led to more pronounced AA oxidation. At the same time, nanoceria has revealed itself as a stronger oxidant in the whole pH range with the highest oxidation ability at pH 6.7 (Fig. 3A). AA oxidation in the presence OV NPs was higher than in control sample (without NPs) only at pH 6.7, while at more alkaline pH the decrease of AA oxidation was observed (Fig. 3B). The process of ascorbic acid oxidation for all concentrations of CeO_{2-x} nanoparticles is more effective at lower pH values, so it should be observed preferably in tumor cells, where pH value is less than in non-tumor ones. As was expected, oxidative ability of OV NPs is sufficiently less due to lower value of standard redox potential of V^{4+}/V^{5+} ionic pair (~1 eV) compared to the one of Ce^{4+}/Ce^{3+} one (~1.66 eV). Higher AA oxidative ability of CeO_{2-x} NPs compared to OV NPs correlates with

higher ascorbyl radical generation ability [31] as well as efficiency of GSH, DTT, and cysteine oxidation by NPs [27].

ROS Generation by CeO_{2-x} and OV Nanoparticles and NPs-based SMC in L929 and T24T Cell Lines

The oxidation of AA by studied NPs is accompanied by $Ce^{4+} \rightarrow Ce^{3+}$ ($V^{5+} \rightarrow V^{4+}$) reduction, which can be followed by re-oxidation of Ce^{3+} and V^{4+} ions by molecular oxygen with formation of superoxide ($O_2 + e^- \rightarrow O_2^{\bullet-}$). Such a process is expected to proceed cyclically via reversible $Ce^{3+} \leftrightarrow Ce^{4+}$ ($V^{4+} \leftrightarrow V^{5+}$) transitions, enabling continuous ROS formation. In Fig. 4 and Fig. 5 the ROS generation processes are compared for CeO_{2-x} and $GdYVO_4:Eu^{3+}$ NPs and NPs-based SMC for L929 (Fig. 4) and T24T (Fig. 5) cell lines including total ROS content (A, B) and specific ROS types ($O_2^{\bullet-}$ – C, D, $^{\bullet}OH$ – E, F). To assess the processes of ROS generation in cells by NPs and NPs-based SMC, DCFDA (2′, 7′-dichlorodihydrofluorescein diacetate), DHE (dihydroethdium), and APF (Aminophenyl fluorescein) probes were used, first of which indicates total level of intracellular ROS, and other ones the level of superoxide and hydroxyl radicals, respectively. While both types of NPs stimulate ROS generation in L929 and T24T cells at AA addition, the efficiency of this process differ sufficiently for different NPs with CeO_{2-x} revealing higher and more sustained ROS generation. This AA-triggered ROS generation effect further increases at incubation with NPs-based SMC. In order to determine whether this increase is related to additive or synergistic effect of the separate components (NPs, AA, cholesterol and K3) of NPs-based SMCs, the values of combination index (CI) [37] were calculated (Fig. S1). Combination index (CI) values below 1 were observed for all AA combinations with CeO_{2-x}, including CeO_{2-x}-based supramolecular complexes (SMC), indicating a synergistic effect over the 72-hour period. In contrast, no synergistic interaction was observed for OV nanoparticle-based SMC (CI > 1). The synergistic effect for CeO_{2-x} NPs-based combinations can be ascribed to superoxide generation at autooxidation of AA enhanced by the NPs, followed by formation of H_2O_2 due to high SOD-like activity of CeO_{2-x} NPs [38]. In this way, menadione and CeO_{2-x} NPs can act in synergistic way producing additional ROS and increasing prooxidant activity of nanoceria.

The AA-triggered generation of specific ROS types ($O_2^{\bullet-}$ - C, D, $^{\bullet}OH$ – E, F) by NPs and NPs-based SMC follows the same pattern as the one for total intracellular ROS. The content of superoxide anions and hydroxyl radicals increased drastically in the presence of AA for both cell lines and both NPs types, but again for CeO_{2-x} NPs NPs and CeO_{2-x} -based SMC this effect was more pronounced. The strong correlation between increases in $O_2^{\bullet-}$ and $^{\bullet}OH$ concentrations observed for both types of NPs allows suggesting the following mechanism of ROS generation: (1) superoxide generation at NPs-catalyzed AA oxidation (involving $Ce^{3+} \leftrightarrow Ce^{4+}$ and $V^{4+} \leftrightarrow V^{5+}$ redox cycling; (2) H_2O_2 formation from superoxide anions which can be enhanced by superoxide dismutase (SOD) – like activity of CeO_{2-x} [38] and OV [36] NPs; (3) $^{\bullet}OH$ generation from H_2O_2 by Fenton-like reaction which can proceed both with participation of NPs themselves and labile iron pool [14]. In this way, superoxide generation by NPs trigger the formation of other ROS types.

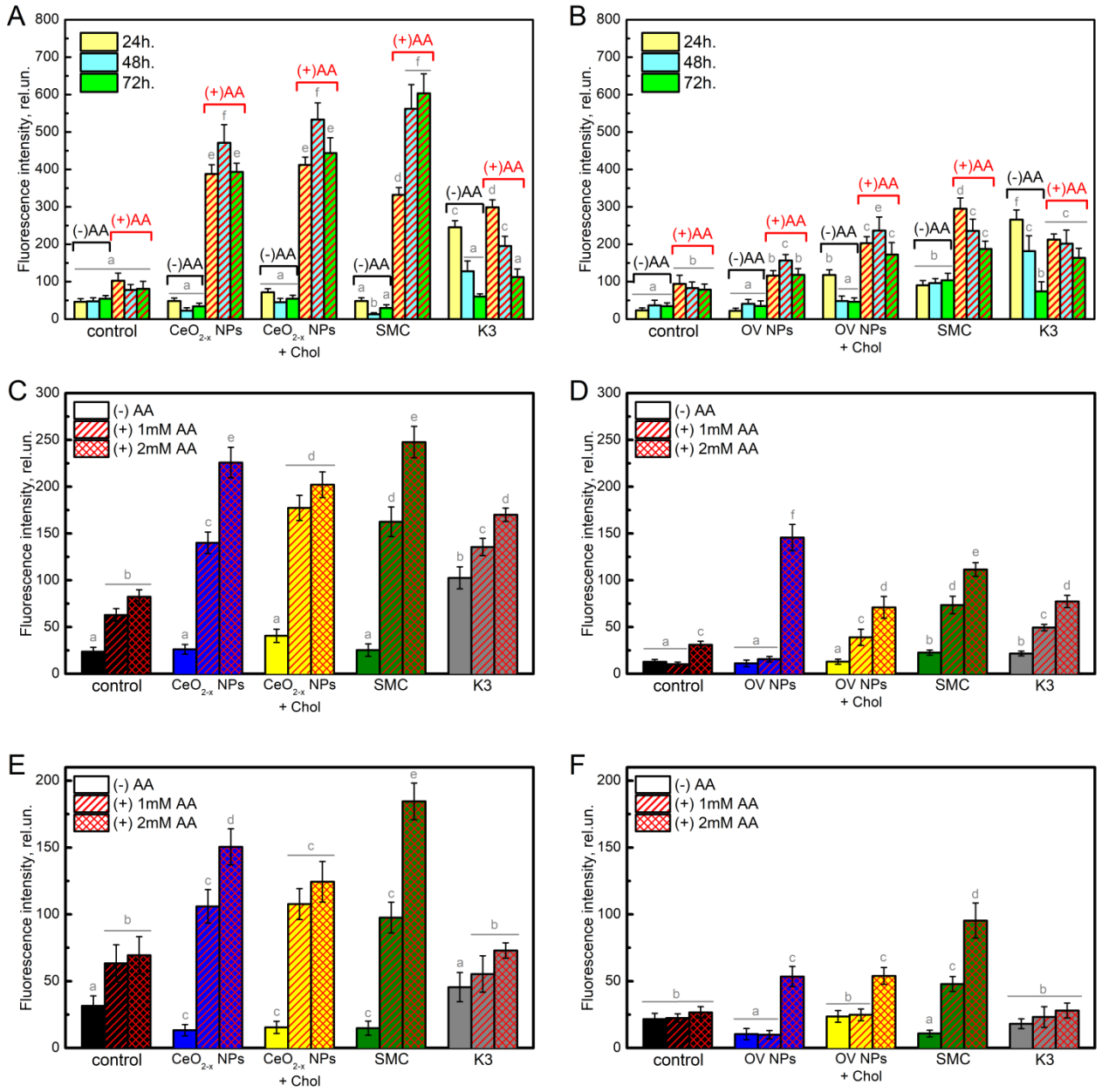


Fig. 4 (A, B) Effect of CeO_{2-x} and $GdYVO_4:Eu^{3+}$ NPs and NPs-based SMC on the total level of intracellular ROS in L929 mouse fibrosarcoma cells; **(C, D)** Effect of CeO_{2-x} and $GdYVO_4:Eu^{3+}$ NPs and NPs-based SMC on the level of intracellular superoxide ($O_2^{\bullet-}$) in L929 mouse fibrosarcoma cells; **(E, F)** Effect of CeO_{2-x} and $GdYVO_4:Eu^{3+}$ NPs and NPs-based SMC on the level of hydroxyl radicals ($^{\bullet}OH$) in L929 mouse fibrosarcoma cells. (+)AA – with ascorbic acid, (-)AA – without ascorbic acid. Different letters (a, b, c, d, e, f) indicate statistically significant differences between groups ($p < 0.05$).

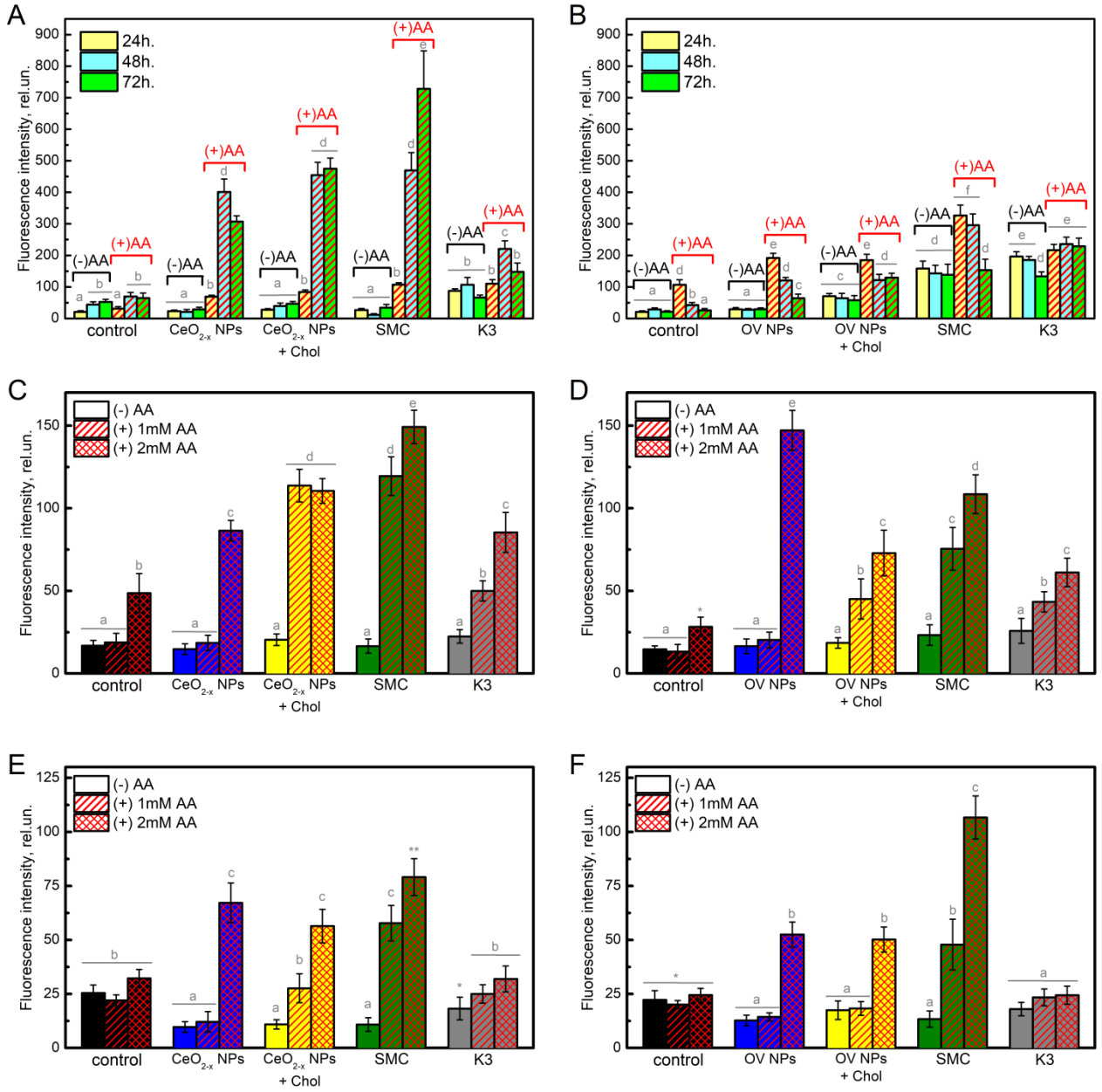


Fig. 5 (A, B) Effect of CeO_{2-x} and $GdYVO_4:Eu^{3+}$ NPs and NPs-based SMC on the total level of intracellular ROS in human bladder cancer (T24T) cells; **(C, D)** Effect of CeO_{2-x} and $GdYVO_4:Eu^{3+}$ NPs and NPs-based SMC on the level of intracellular superoxide ($O_2^{\bullet-}$) in human bladder cancer (T24T) cells; **(E, F)** Effect of CeO_{2-x} and $GdYVO_4:Eu^{3+}$ NPs and NPs-based SMC on the level of hydroxyl radicals ($^{\bullet}OH$) in human bladder cancer (T24T) cells. (+)AA – with ascorbic acid, (-)AA – without ascorbic acid. Different letters (a, b, c, d, e, f) indicate statistically significant differences between groups ($p < 0.05$).

Effect of CeO_{2-x} and OV Nanoparticles and NPs-based SMC on the Cellular Antioxidant Defense and Energy Metabolism in L929 and T24T Cell Lines

To assess the impact of NPs and NPs-based SMCs on the antioxidant defense system and energy metabolism of L929 and T24T cancer cells, we have studied several biochemical markers associated with oxidative stress progression and physiological

state of cancer cell including the GSH/GSSG ratio, 8-isoprostane level, and ATP level (Fig. 6 for L929 and Fig. 7 for T24T cell lines) in the presence of NPs and NPs-based SMC.

Enhanced ROS generation observed in L929 and T24T cell lines shown in Fig. 4 and Fig. 5 alone may not be sufficient to ensure effective cancer cell elimination as cancer cells produce higher levels of ROS by themselves due to rapid metabolism and mitochondrial dysfunction. Elevated level of reduced glutathione (GSH) in cancer cells helps buffering the oxidative stress preventing damage to DNA, proteins, and lipids [3]. Therefore, the ratio of reduced and oxidized glutathione (GSH/GSSG ratio) is a key parameter of cellular redox balance. In Fig. 6 (A, B) and Fig. 7 (A, B) the effect of CeO_{2-x} and $GdYVO_4:Eu^{3+}$ NPs and NPs-based SMC for L929 (Fig. 6) and T24T (Fig. 7) cell lines is shown. Importantly, the studied NPs and NPs-based SMC not just increase the ROS content in the cells, but also deplete the pool of reduced glutathione decreasing the antioxidant capability of the cells. The effect of glutathione depletion caused by high DHA intake by cancer cells with enhanced GLUT1 expression was described previously [39], so for L929 and T24T cancer cell lines we observe the combined effect provided by oxidized AA itself and ROS generated by NPs as a result of AA oxidation on the glutathione pool. The most sufficient GSH/GSSG decrease, as well as the most sufficient effect of AA for both cell lines was observed for CeO_{2-x}-based SMC.

As a result of enhanced ROS generation under conditions of reduced glutathione depletion, AA-triggered ROS generation by NPs and NPs-based SMCs induced a severe oxidative stress significant increase in the level of 8-isoprostane, a well-known marker of lipid peroxidation and membrane damage (Fig. 6 (C, D) for L929 cell line and Fig. 7 (C, D) for T24T cell line).

High ATP levels in cancer cells compared to normal ones stimulate their rapid proliferation, survival, and chemoresistance [40]. Analysis of intracellular ATP levels in the presence of NPs and NPs-based SMC revealed marked suppression of cellular energy metabolism. Effect of ATP depletion at AA addition was most pronounced for CeO_{2-x}-based SMCs. Since ATP depletion is commonly associated with irreversible cellular damage and activation of programmed cell death pathways, these results strongly support the proposed ROS-mediated anticancer mechanism of the studied NPs and NPs-based SMC. Decreased ATP production can be caused by ROS-induced oxidative damage to mitochondria.

Generally, CeO_{2-x} NPs and especially CeO_{2-x}-based SMCs produced stronger effects on the values of GSH/GSSG ratio, 8-isoprostane level, and ATP level compared to OV-based systems in full agreement with higher ROS generating activity of nanoceria stimulated by AA. In the absence of AA, the observed changes were considerably weaker demonstrating the key role of efficiency of AA-triggered redox cycling in general effect on the antioxidant defense system of the both lines of cancer cells.

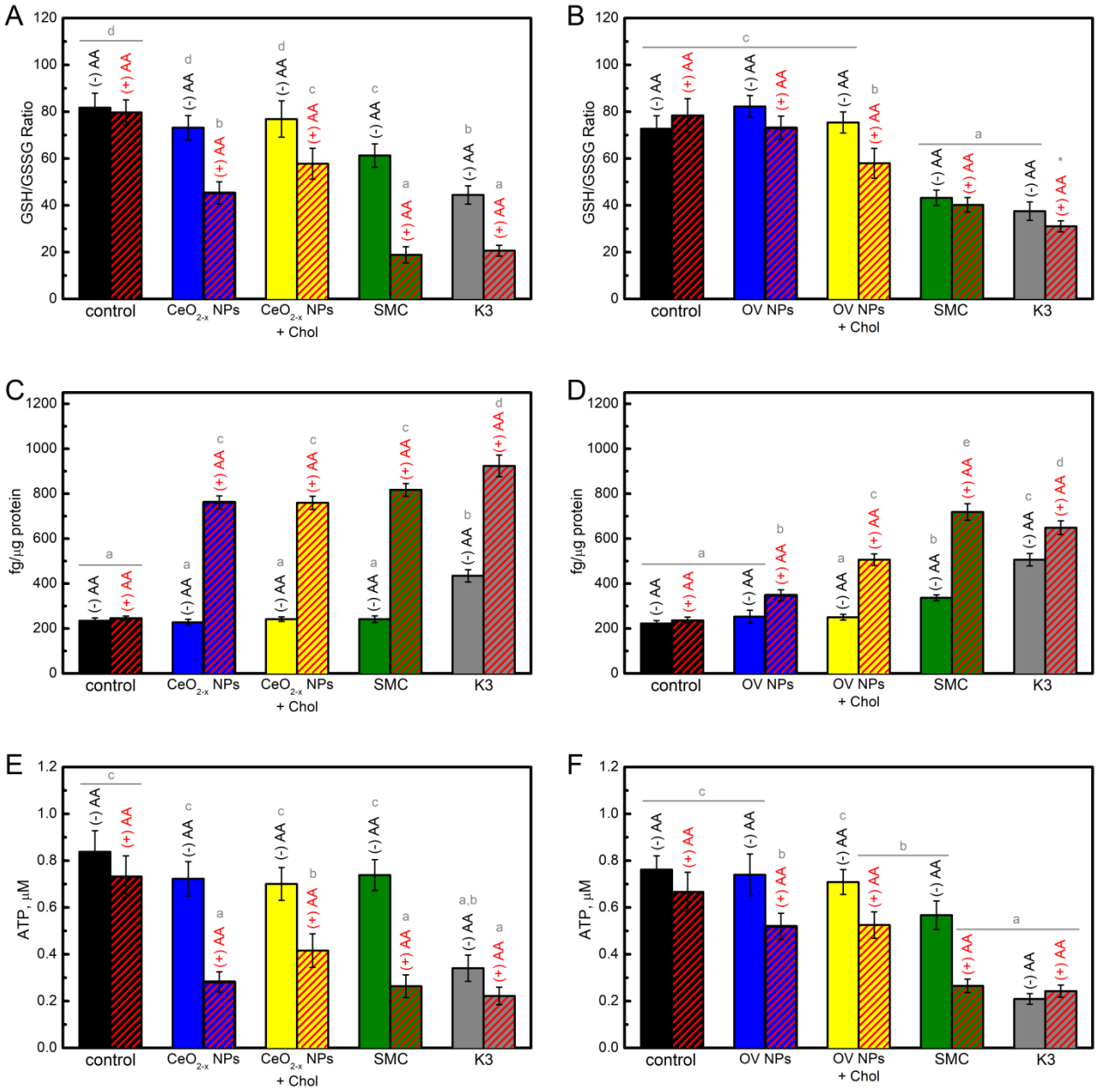


Fig. 6 (A, B) Effect of CeO_{2-x} and $GdYVO_4:Eu^{3+}$ NPs and NPs-based SMC on the GSH/GSSG ratio in L929 mouse fibrosarcoma cells; **(C, D)** Effect of CeO_{2-x} and $GdYVO_4:Eu^{3+}$ NPs and NPs-based SMC on the level of 8-isoprostane in L929 mouse fibrosarcoma cells; **(E, F)** Effect of CeO_{2-x} and $GdYVO_4:Eu^{3+}$ NPs and NPs-based SMC on the ATP level in L929 mouse fibrosarcoma cells. (+)AA – with ascorbic acid, (-)AA – without ascorbic acid. Different letters (a, b, c, d, e, f) indicate statistically significant differences between groups ($p < 0.05$).

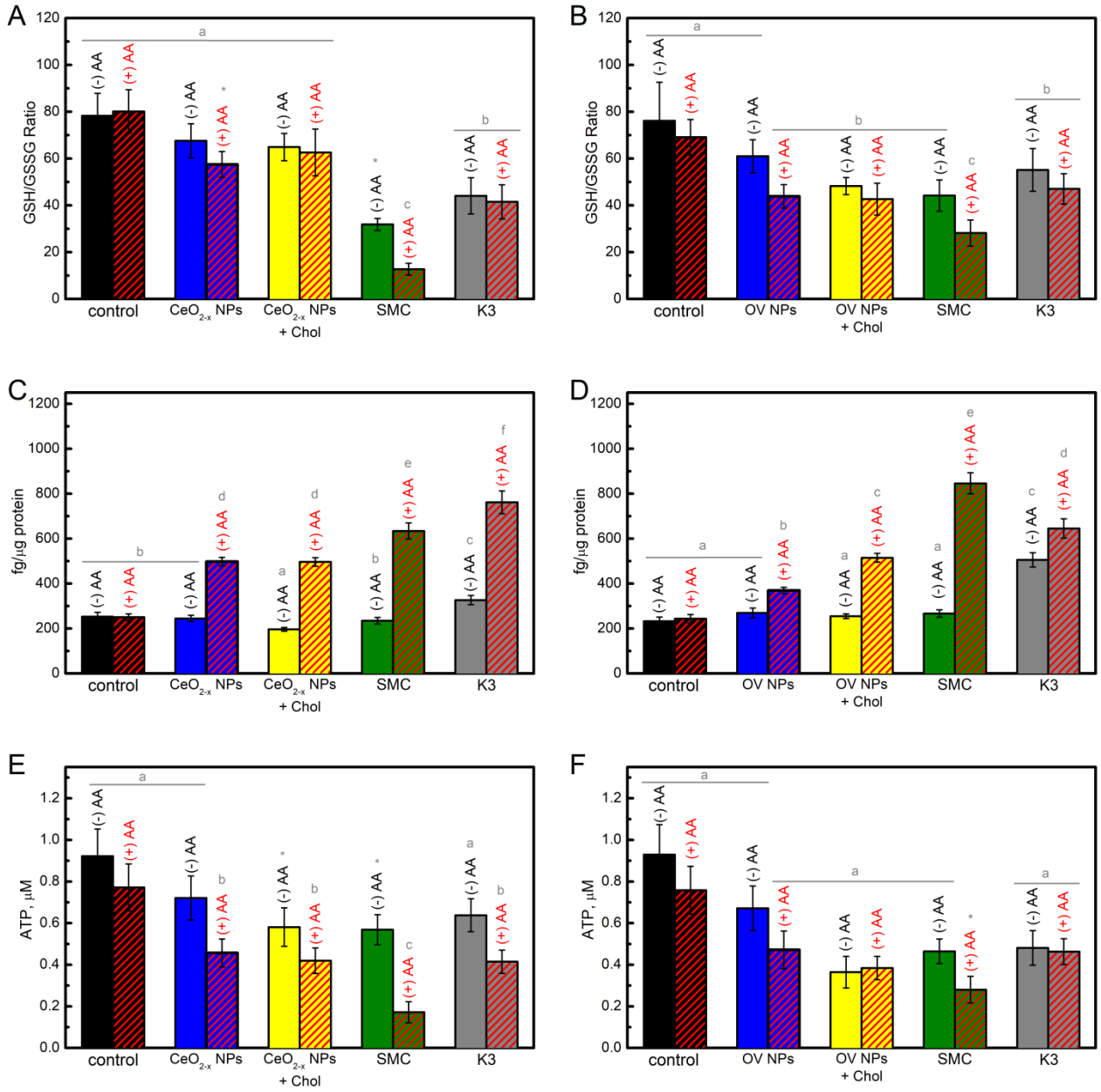


Fig. 7 (A, B) Effect of CeO_{2-x} and $GdYVO_4:Eu^{3+}$ NPs and NPs-based SMC on the GSH/GSSG ratio in human bladder cancer (T24T) cells; **(C, D)** Effect of CeO_{2-x} and $GdYVO_4:Eu^{3+}$ NPs and NPs-based SMC on the level of 8-isoprostane in human bladder cancer (T24T) cells; **(E, F)** Effect of CeO_{2-x} and $GdYVO_4:Eu^{3+}$ NPs and NPs-based SMC on the ATP level in human bladder cancer (T24T) cells. (+)AA – with ascorbic acid, (-)AA – without ascorbic acid. Different letters (a, b, c, d, e, f) indicate statistically significant differences between groups ($p < 0.05$).

Effects of CeO_{2-x} and OV NPs and NPs-based SMC on Mitochondrial Dysfunction and Apoptosis in L929 and T24T Cell Lines

Since mitochondrial dysfunction is one of the major consequences of ROS overproduction, mitochondrial membrane potential and caspase-3 activation were analyzed as indicators of oxidative stress-induced programmed cell death.

The effect of NPs and NPs-based SMC on the loss of mitochondrial depolarization processes was confirmed using JC-1 probe which is a commonly used tool for studying mitochondrial membrane potential (MMP). At high MMP, JC-1 predominantly forms J-aggregates that emit red fluorescence at 590 nm, whereas decrease of MMP leads to disaggregation and formation of monomers displaying green fluorescence at 510 nm. The decrease of fluorescence intensity of JC-1 J-aggregates (Fig. 8 (A, B) and Fig. 9 (A, B)) with simultaneous increase of the ratio of green (monomer) to red (aggregate) fluorescence (Fig. 8 (C, D) and Fig. 9 (C, D)) for NPs and NPs-based SMC at AA addition clearly indicate mitochondrial depolarization and reflect a substantial decrease in mitochondrial activity. The effect of MMP decrease allows confirming the ROS-induced functional decline of mitochondria. The abovementioned ATP depletion can be viewed as a direct result of this process.

The loss of MMP is usually closely associated to caspase-3 activity, which is a critical executioner protease in the apoptotic pathway. In Fig. 8 (A, B) and Fig. 9 (A, B) the effect of CeO_{2-x} and $GdYVO_4:Eu^{3+}$ NPs and NPs-based SMC for L929 (Fig. 8) and T24T (Fig. 9) cell lines on the caspase-3 level is shown. The sufficient increase of caspase-3 activity for both types of NPs and cells which can be seen visually in Fig. 10 confirms the induction of apoptic processes by NPs and SMCs in the presence of AA.

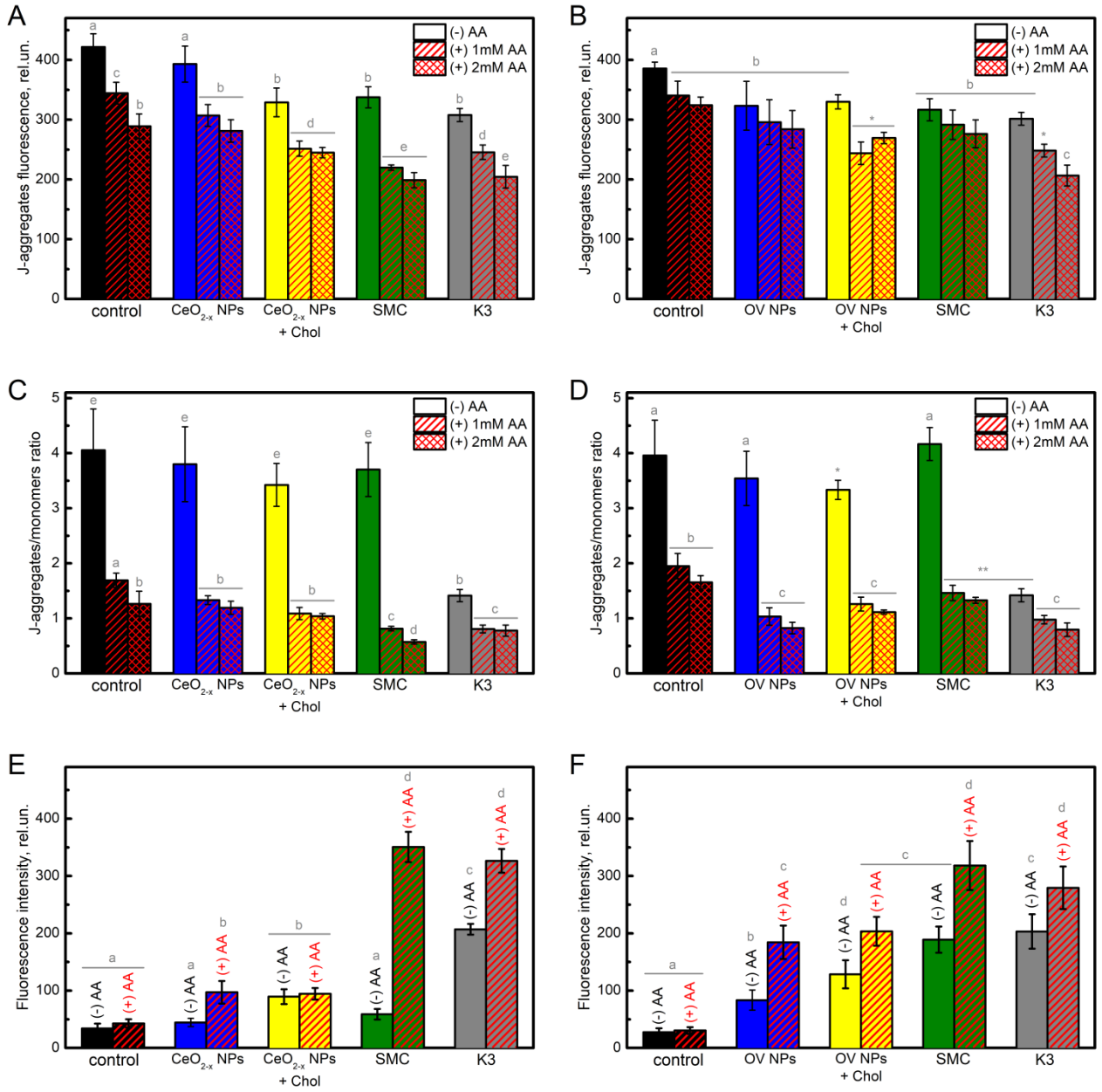


Fig. 8 (A, B) Effect of CeO_{2-x} and $GdYVO_4:Eu^{3+}$ NPs and NPs-based SMC on the mitochondrial membrane potential (determined by JC-1 J-aggregate band) in L929 mouse fibrosarcoma cells; **(C, D)** Effect of CeO_{2-x} and $GdYVO_4:Eu^{3+}$ NPs and NPs-based SMC on the mitochondrial membrane potential (determined by JC-1 monomer/J-aggregate band ratio) in L929 mouse fibrosarcoma cells; **(E, F)** Effect of CeO_{2-x} and $GdYVO_4:Eu^{3+}$ NPs and NPs-based SMC on the activity of caspase-3 in L929 mouse fibrosarcoma cells. (+)AA – with ascorbic acid, (-)AA – without ascorbic acid. Different letters (a, b, c, d, e, f) indicate statistically significant differences between groups ($p < 0.05$).

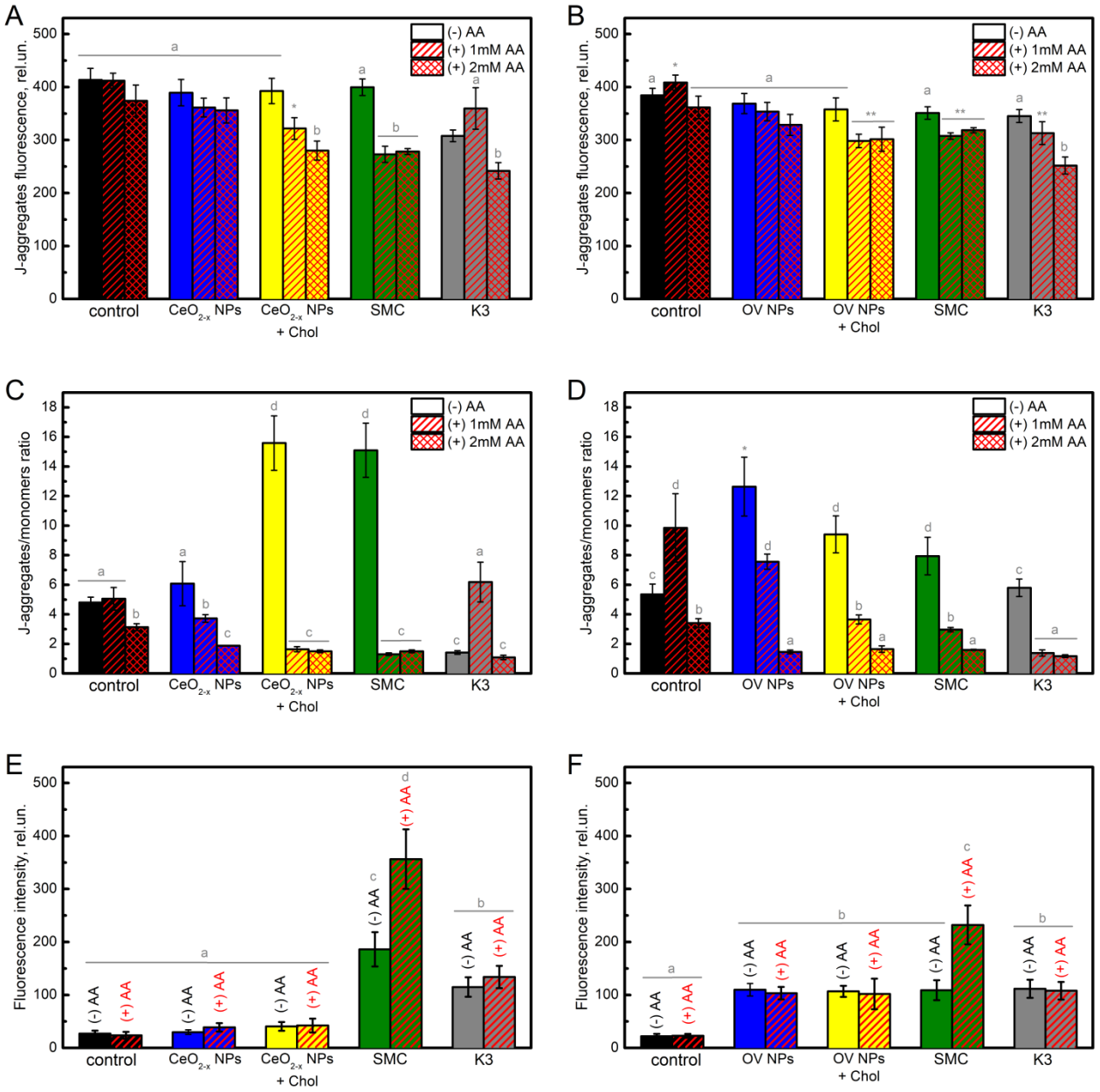


Fig. 9 (A, B) Effect of CeO_{2-x} and $GdYVO_4:Eu^{3+}$ NPs and NPs-based SMC on the mitochondrial membrane potential (determined by JC-1 J-aggregate band) in human bladder cancer (T24T) cells; **(C, D)** Effect of CeO_{2-x} and $GdYVO_4:Eu^{3+}$ NPs and NPs-based SMC on the mitochondrial membrane potential (determined by JC-1 monomer/J-aggregate band ratio) in human bladder cancer (T24T) cells; **(E, F)** Effect of CeO_{2-x} and $GdYVO_4:Eu^{3+}$ NPs and NPs-based SMC on the activity of caspase-3 in human bladder cancer (T24T) cells. (+)AA – with ascorbic acid, (-)AA – without ascorbic acid. Different letters (a, b, c, d, e, f) indicate statistically significant differences between groups ($p < 0.05$).

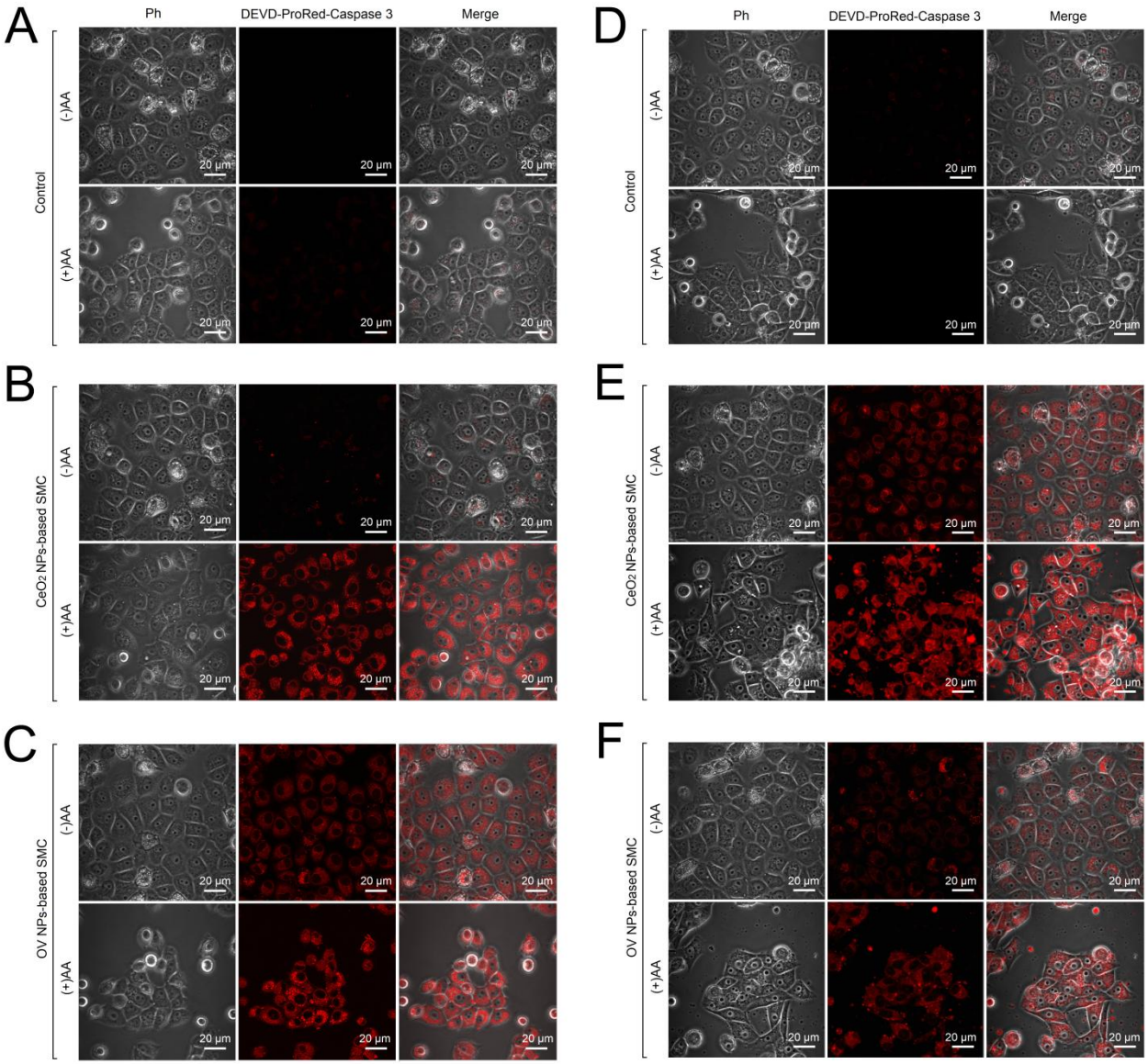


Fig. 10 Effect of CeO_{2-x} and $GdYVO_4:Eu^{3+}$ NPs and NPs-based SMC on the activity of caspase-3 in L929 **(A-C)** and T24T **(D-F)** cells seen as a change of fluorescence intensity of ProRed™ fluorophore (*Caspase Multiplex Activity Assay Fluorometric Kit*).

Effects of CeO_{2-x} and OV NPs and NPs-based SMC on the Viability of L929 and T24T Cell Lines

Finally, the general effect of NPs and NPs-based SMC on the viability of L929 and T24T cell lines was studied by Calcein AM assay. This method uses a non-fluorescent, membrane-permeant Calcein AM dye which turns into strongly fluorescent calcein dye inside living cells through intracellular hydrolysis of AM group by esterases. A decrease in green fluorescence signals a reduction in intracellular esterase activity, which correlates with cell death or compromised physiological states. The effect of CeO_{2-x} and $GdYVO_4:Eu^{3+}$ NPs and NPs-based SMC on the viability of L929 mouse fibrosarcoma cells and T24T human bladder cancer cells is shown in the Fig. 11.

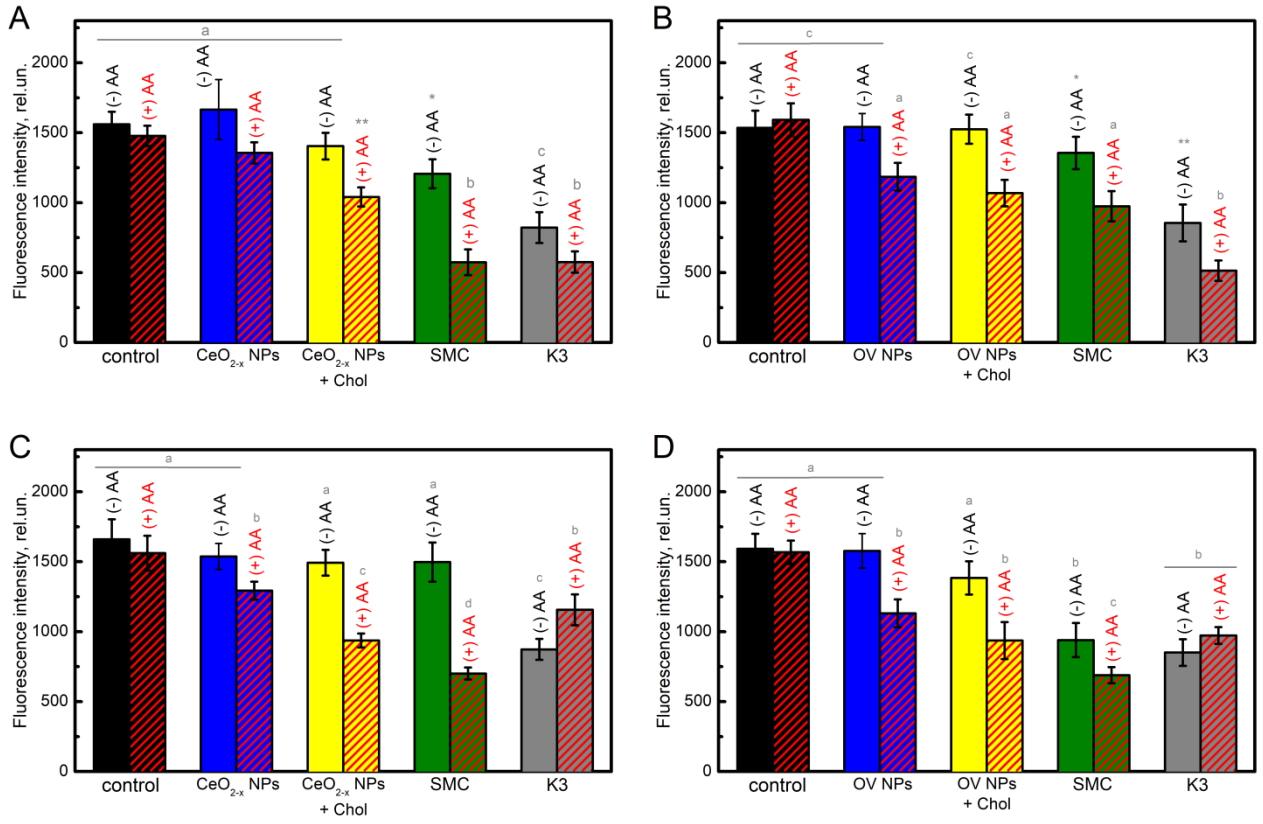


Fig. 11 (A, B) Effect of CeO_{2-x} and $GdYVO_4:Eu^{3+}$ NPs and NPs-based SMC on the viability of L929 mouse fibrosarcoma cells; **(C, D)** Effect of CeO_{2-x} and $GdYVO_4:Eu^{3+}$ NPs and NPs-based SMC on the viability of human bladder cancer (T24T) cells. The viability was determined by Calcein AM assay. (+)AA – with ascorbic acid, (-)AA – without ascorbic acid. Different letters (a, b, c, d, e, f) indicate statistically significant differences between groups ($p < 0.05$).

The sufficient decrease of viability of both types of cells is observed for NPs and NPs-based SMC in the presence of AA with the highest effect for CeO_{2-x}-based SMC (more than two times compared to control and AA in the absence of NPs). At the same time, the effect of OV NPs and OV-based SMC was more moderate.

Discussion

As was reported previously, L929 (mouse fibrosarcoma) and T24/T24T (human bladder carcinoma) cell lines are highly sensitive to pharmacological concentrations of ascorbic acid (AA, typically 1–20 mM), which effect enhances sufficiently in the presence of redox cycling agents such as vitamin K3 (menadione) [31]. The dominant mechanism of AA cytotoxicity in these cells is generally attributed to extracellular oxidation of AA, leading to formation of hydrogen peroxide (H_2O_2), which diffuses into cells and induces oxidative stress. This effect results in glutathione (GSH) depletion, increased reactive oxygen species (ROS), inhibition of glycolytic enzymes such as GAPDH, disruption of cellular energetics, and ultimately cell death.

The experimental results shown in this paper clearly indicate that CeO_{2-x} and $GdYVO_4:Eu^{3+}$ NPs and NPs-based SMC enhance sufficiently the effect of AA on physiological state and antioxidant defense system of L929 and T24T cancer cells. At the same time, as was shown in our previous studies on fibroblasts [31], no cytotoxic

action of CeO_{2-x} NPs and NPs-based SMC was observed for non-tumor cells indicating a preferential cytotoxicity toward cancer cells. This selectivity may be attributed, at least in part, to more efficient AA oxidation and ROS generation at mildly acidic pH values of the tumor microenvironment compared to normal cells. In addition, enhanced susceptibility of cancer cells to oxidative stress, as well as increased uptake of dehydroascorbic acid (DHA) via glucose transporters associated with glycolytic metabolism can also contribute to the observed effects.

The more pronounced ability of cerium oxide (CeO_{2-x}) nanoparticles to oxidize ascorbic acid compared to OV nanoparticles is likely determined by lower value of standard redox potential of V^{4+}/V^{5+} ionic pair (~1 eV) compared to the one of Ce^{4+}/Ce^{3+} one (~1.66 eV) as well as by the differences in surface electron-transfer kinetics and the capacity to sustain catalytic redox cycling. Nanoceria exhibits a highly dynamic Ce^{3+}/Ce^{4+} redox couple that is intrinsically linked to oxygen vacancies and a high density of surface defects, enabling efficient electron exchange between the nanoparticle surface, molecular oxygen, and organic electron donors. Ascorbate can interact with the CeO_{2-x} surface and undergo one-electron oxidation to form the ascorbyl radical, while Ce^{3+} is readily reoxidized by dissolved oxygen, supporting continuous catalytic turnover and promoting the generation of reactive oxygen species. In contrast, in OV nanoparticles, vanadium is incorporated into a relatively rigid VO_4 tetrahedral framework, which limits the accessibility of redox-active sites and slows interfacial electron transfer. Although V^{5+}/V^{4+} transitions can be observed at interaction with various oxidizing/reducing agents [36], the kinetics in the solid-state lattice are less favorable compared to the defect-rich surface of nanoceria. In addition, orthovanadates generally exhibit lower electronic conductivity and a lower density of surface defects, further constraining efficient electron transfer from ascorbate. Thus, the combination of high surface defectivity, rapid Ce^{3+}/Ce^{4+} cycling, and effective coupling to oxygen reduction underlies the superior pro-oxidant activity of nanoceria toward AA.

Similar to AA-triggered redox cycling of menadione accompanied by ROS generation, AA-induced $Ce^{3+}\leftrightarrow Ce^{4+}$ and $V^{4+}\leftrightarrow V^{5+}$ redox cycling in CeO_{2-x} and $GdYVO_4:Eu^{3+}$ NPs, respectively, stimulates superoxide generation from molecular oxygen. The AA-triggered ROS burst, in turn, causes a depletion of reduced glutathione, stimulates oxidation of biological membranes, and decreases mitochondrial potential compromising the viability of cancer cells. While the similar mechanism of prooxidant activity can be suggested for both NPs, more efficient redox properties of $Ce^{3+}\leftrightarrow Ce^{4+}$ ions in nanoceria (which correlates with higher redox potential of the Ce^{4+}/Ce^{3+} pair), determines that all the indicators from efficiency of ROS generation to decrease of cell viability for CeO_{2-x} NPs exceed the ones observed for $GdYVO_4:Eu^{3+}$ NPs. At the same time, these results clearly show the generality of the anticancer effects previously observed for nanoceria-based SMC and confirm the role of AA-induced redox cycling in inorganic NP as a key mechanism for highly selective cancer treatment.

Summarizing, the mechanism of AA-triggered antitumor action of NPs and their cholesterol complexes with menadione include: 1) oxidation of AA by CeO_{2-x} and $GdYVO_4:Eu^{3+}$ NPs with simultaneous formation of superoxide anions; 2) formation of H_2O_2 from superoxide due to SOD-like activity of NPs followed by

Fenton-like •OH generation inside tumor cells; 3) depletion of intracellular thiols due to combined effect provided by DHA, and ROS generated by NPs in the (1) and (2) stages; 4) violation of oxidative phosphorylation processes as a result of ROS action on mitochondria leading to significant decrease in the ATP concentration; 5) triggering cell death by apoptosis with significant increase in the activity of caspase-3 as a result of oxidative stress. The studies reveal common mechanisms of action of SMC for both tumor lines (L929 and T24T). Despite more efficient OV penetration into both types of cancer cells, the antitumor effect is more pronounced for nanoceria-based SMC than for OV-based SMC. This superiority of nanoceria and nanoceria-based SMC can be related to higher values of Ce^{3+}/Ce^{4+} pair redox potential compared with the one for V^{4+}/V^{5+} pair making oxidation of AA and other biomolecules more efficient. The main features of the AA-triggered cytotoxic action of bare nanoceria and OV NPs and NPs-based SMC are ROS generation, reduction of antioxidant potential, disruption of mitochondrial function and initiation of proapoptotic processes. The revealed patterns of action in tumor cells of different lines indicate universal mechanisms of influence of synthesized SMC and their prospects for the development of antitumor therapeutic agents.

Conclusions

CeO_{2-x} nanoparticles synergistically enhance the anticancer activity of ascorbic acid in L929 fibrosarcoma and T24T metastatic bladder cancer cells due to $Ce^{3+}\leftrightarrow Ce^{4+}$ redox cycling and high ROS-generating capability. In contrast, OV nanoparticles and OV-based combinations exhibited lower antitumor efficacy, with no evidence of synergistic interaction. AA-induced redox cycling in the nanoparticles stimulated ROS generation accompanied by glutathione depletion, lipid peroxidation, mitochondrial dysfunction, ATP depletion, caspase-3 activation, and decreased cancer cell viability. Incorporation of nanoparticles into cholesterol/menadione-based supramolecular complexes further enhances oxidative stress and cytotoxicity, with a synergistic effect observed for CeO_{2-x}-based SMCs. Similar effects observed in both L929 and T24T cell lines indicate a general ROS-mediated mechanism of anticancer activity. The obtained results show that AA-triggered redox-active agents, particularly nanoceria-based SMCs are promising candidates for highly selective ROS-based anticancer therapy.

Acknowledgments

The murine L929 cells and fibroblasts were kindly provided by the Institute for Problems of Cryobiology and Cryomedicine of the National Academy of Sciences of Ukraine.

The authors are very grateful to Dr. Kateryna Hubenko, Dr. Martin Hantusch and Steffi Kaschube for their help with the XPS measurements, and to Dr. Olga Vashchenko from the Institute for Scintillation Materials, National Academy of Sciences of Ukraine for her help with DSC. The murine L929 cells were kindly provided by the Institute for Problems of Cryobiology and Cryomedicine of the National Academy of Sciences of Ukraine.

Author Contributions All authors contributed to the study conception and design. Nanoparticles and SMC were obtained by O. S. and V. K. Experiments and analysis of experimental data were

done by N. K., G. D., and Y. K. The first draft of the manuscript was written by V. S. with assistance of P. M. and S. Y. All authors read and approved the final manuscript.

Funding This research was supported by National Research Foundation of Ukraine, Grant № 2023.03/0050.

Data Availability The datasets generated during and/or analyzed during the current study are available from the corresponding authors on reasonable request.

Conflict of interest The authors declare no conflicts of interest

References

1. Yang, B., Chen, Y., Shi, J. (2019). Reactive oxygen species (ROS)-based nanomedicine. *Chemical Reviews*, 119, 4881–4985. https://doi.org/10.1021/acs.chemrev.8b00626
2. Bellezza, I., Mierla, A.L., Minelli, A. (2010). Nrf2 and NF-κB and their concerted modulation in cancer pathogenesis and progression. *Cancers*, 2, 483–497. https://doi.org/10.3390/cancers2020483
3. Estrela, J.M., Ortega, A., Obrador, E. (2006). Glutathione in cancer biology and therapy. *Critical Reviews in Clinical Laboratory Sciences*, 43, 143–181. https://doi.org/10.1080/10408360500523878
4. Sadikovic, B., Al-Romaih, K., Squire, J.A., Zielenska, M. (2008). Cause and consequences of genetic and epigenetic alterations in human cancer. *Current Genomics*, 9, 394–408. https://doi.org/10.2174/138920208785699580
5. Zhang, Q., Luo, Q., Liu, Z., Sun, M., Dong, X. (2023). Nano-ROS-generating approaches to cancer dynamic therapy: Lessons from nanoparticles. *Chemical Engineering Journal*, 457, 141225. https://doi.org/10.1016/j.cej.2022.141225
6. Wang, J., Yi, J. (2008). Cancer cell killing via ROS: to increase or decrease, that is the question. *Cancer Biology & Therapy*, 7, 1875–1884. https://doi.org/10.4161/cbt.7.12.7067
7. Reang, J., Sharma, P.C., Thakur, V.K., Majeed, J. (2021). Understanding the therapeutic potential of ascorbic acid in the battle to overcome cancer. *Biomolecules*, 11, 1130. https://doi.org/10.3390/biom11081130
8. Vissers, M.C., Das, A.B. (2018). Potential mechanisms of action for vitamin C in cancer: reviewing the evidence. *Frontiers in Physiology*, 9, 809. https://doi.org/10.3389/fphys.2018.00809
9. Frei, B., Lawson, S. (2008). Vitamin C and cancer revisited. *Proceedings of the National Academy of Sciences*, 105, 11037–11038. https://doi.org/10.1073/pnas.0806433105
10. Beck, R., Verrax, J., Dejeans, N., Taper, H., Calderon, P.B. (2009). Menadione reduction by pharmacological doses of ascorbate induces an oxidative stress that kills breast cancer cells. *International Journal of Toxicology*, 28, 33–42. https://doi.org/10.1177/1091581809333139
11. Ren, X., Santhosh, S.M., Coppo, L., Ogata, F.T., Lu, J., Holmgren, A. (2019). The combination of ascorbate and menadione causes cancer cell death by oxidative stress and replicative stress. *Free Radical Biology and Medicine*, 134, 350–358. https://doi.org/10.1016/j.freeradbiomed.2019.01.037
12. Lasheras, J., Jamison, J.M., Summers, J.L. (2008). A 12 week, open label, phase I/IIa study using apatone for the treatment of prostate cancer patients who have failed standard therapy. *International Journal of Medical Sciences*, 5, 62–67. https://doi.org/10.7150/ijms.5.62

13. Gilloteaux, J., Lau, H.L., Gourari, I., Neal, D., Jamison, J.M., Summers, J.L. (2015). Apatone® induces endometrioid ovarian carcinoma (MDAH 2774) cells to undergo karyolysis and cell death by autoschizis: A potent and safe anticancer treatment. *Translational Research in Anatomy*, 1, 25–39. https://doi.org/10.1016/j.tria.2015.10.005
14. Ge, P., Tao, X., Qu, J., et al. (2026). A comprehensive review of vitamin C for cancer therapy: Anti-tumor mechanisms and nano-formulation strategies. *International Journal of Nanomedicine*, 1, 1–29. https://doi.org/10.2147/IJN.S559426
15. Huang, Y., Ren, J., Qu, X. (2019). Nanozymes: classification, catalytic mechanisms, activity regulation, and applications. *Chemical Reviews*, 119, 4357–4412. https://doi.org/10.1021/acs.chemrev.8b00672
16. Pal, S, Jana, NR (2020). Pharmacologic vitamin C-based cell therapy via iron oxide nanoparticle-induced intracellular Fenton reaction. *ACS Applied Nano Materials*, 3, 1683–1692. https://doi.org/10.1021/acsanm.9b02405
17. An, Q., Sun, C., Li, D., Xu, K., Guo, J., Wang, C. (2013). Peroxidase-like activity of Fe_3O_4@carbon nanoparticles enhances ascorbic acid-induced oxidative stress and selective damage to PC-3 prostate cancer cells. *ACS Applied Materials & Interfaces*, 5, 13248–13257. https://doi.org/10.1021/am4042367
18. Li, T., He, F., Liu, B., et al. (2020). In situ synthesis of FeOCl in hollow dendritic mesoporous organosilicon for ascorbic acid-enhanced and MR imaging-guided chemodynamic therapy in neutral pH conditions. *ACS Applied Materials & Interfaces*, 12, 56886–56897. https://doi.org/10.1021/acsami.0c19330
19. Yi, Z., Yang, X., Liang, Y., Tong, S. (2024). Iron oxide nanozymes enhanced by ascorbic acid for macrophage-based cancer therapy. *Nanoscale*, 16, 14330–14338. https://doi.org/10.1039/D4NR01208A
20. Tsymbal, S.A., Moiseeva, A.A., Agadzhanian, N.A., et al. (2021). Copper-containing nanoparticles and organic complexes: metal reduction triggers rapid cell death via oxidative burst. *International Journal of Molecular Sciences*, 22, 11065. https://doi.org/10.3390/ijms222011065
21. Shen, Q., Zhu, X., Huo, M., et al. (2025). A hollow nanozyme-based multifunctional platform enhances sonodynamic-chemodynamic-induced ferroptosis for cancer therapy. *RSC Advances*, 15, 9408–9419. https://doi.org/10.1039/D5RA00032G
22. Ren, G., Lu, M., Zhao, Z., et al (2023). Cobalt single-atom nanozyme co-administration with ascorbic acid enables redox imbalance for tumor catalytic ablation. *ACS Biomaterials Science & Engineering*, 9, 1066–1076. https://doi.org/10.1021/acsbiomaterials.2c01301
23. Chong, Y., Dai, X., Fang, G., et al. (2018). Palladium concave nanocrystals with high-index facets accelerate ascorbate oxidation in cancer treatment. *Nature Communications*, 9, 4861. https://doi.org/10.1038/s41467-018-07257-z
24. Tang, J.L., Moonshi, S.S., Ta, H.T. (2023). Nanoceria: An innovative strategy for cancer treatment. *Cellular and Molecular Life Sciences*, 80, 46. https://doi.org/10.1007/s00018-023-04694-y
25. Efunnuga, A., Efunnuga, A., Onivefu, A.P., Ifijen, I.H., Maliki, M., Omorogbe, S.O., Olugbemide, A.D. (2024). Nanomedicine advancements: vanadium oxide nanoparticles as a game-changer in antimicrobial and anticancer therapies. *BioNanoScience*, 14, 3715–3756. https://doi.org/10.1007/s12668-024-01566-y
26. Rollin-Genetet, F., Seidel, C., Artells, E., Auffan, M., Thiéry, A., Vidaud, C. (2015). Redox reactivity of cerium oxide nanoparticles induces the formation of disulfide bridges in thiol-

containing biomolecules. *Chemical Research in Toxicology*, 28, 2304–2312. https://doi.org/10.1021/acs.chemrestox.5b00319

27. Kavok, N.S., Dudetskaya, G.V., Seminko, V.V., et al. (2025). Influence of redox cyclers on thiol oxidation in the presence of nanoparticles. *Biophysical Bulletin*, 53, 7–17. https://doi.org/10.26565/2075-3810-2025-53-01
28. Ibañez, I.L., Notcovich, C., Catalano, P.N., Bellino, M.G., Durán, H. (2015). The redox-active nanomaterial toolbox for cancer therapy. *Cancer Letters*, 359, 9–19. https://doi.org/10.1016/j.canlet.2015.01.013
29. Lauridsen, A.R., Skorda, A., Winther, N.I., Bay, M.L., Kallunki, T. (2024). Why make it if you can take it: review on extracellular cholesterol uptake and its importance in breast and ovarian cancers. *Journal of Experimental & Clinical Cancer Research*, 43, 254. https://doi.org/10.1186/s13046-024-03172-y
30. Eilenberger, C., Selinger, F., Rothbauer, M., Lin, Y., Limbeck, A., Schädl, B., Grillari, J., Kavok, N., Klochkov, V., Malyukin, Y., Margitich, V., Ertl, P. (2021). Cytotoxicity, retention, and anti-inflammatory effects of a CeO_2 nanoparticle-based supramolecular complex in a 3D liver cell culture model. *ACS Pharmacology & Translational Science*, 4, 101-106. https://doi.org/10.1021/acsptsci.0c00170
31. Goltsev, A.N., Babenko, N.N., Gaevskaya, A., Chelombitko, O.V., Bondarovich, N.A., Dubrava, T.G., Ostankov, M.V., Klochkov, V.K., Kavok, N.S., Malyukin, Y.V. (2015). Functional activity of Ehrlich carcinoma cells after treatment with hybrid nanocomplexes containing orthovanadates of rare-earth elements, cholesterol and luminescent dye. *Fiziolohichnyi zhurnal*, 61, 60-68. https://doi.org/10.15407/fz61.06.060
32. Kavok, N., Dudetskaya, G., Seminko, V., et al. (2025). Ascorbate-triggered antitumor activity of nanoceria- and ceria-based supramolecular complexes in 2D and 3D cell cultures. *ACS Applied Bio Materials* 8:9730–9740. https://doi.org/10.1021/acsabm.5c00916
33. Jin, H., Yu, Y., Hu, Y., et al. (2014). Divergent behaviors and underlying mechanisms of cell migration and invasion in non-metastatic T24 and its metastatic derivative T24T bladder cancer cell lines. *Oncotarget*, 6, 522. https://doi.org/10.18632/oncotarget.2680
34. Ferreira, E., Ferreira, D., Relvas-Santos, M., et al. (2024). Aberrantly glycosylated GLUT1 as a poor prognosis marker in aggressive bladder cancer. *International Journal of Molecular Sciences*, 25, 3462. https://doi.org/10.3390/ijms25063462
35. Gilloteaux, J., Jamison, J.M., Arnold, D., Taper, H.S., Summers, J.L. (2001). Ultrastructural aspects of autoschizis: a new cancer cell death induced by the synergistic action of ascorbate/menadione on human bladder carcinoma cells. *Ultrastructural Pathology*, 25, 183–192. https://doi.org/10.1080/019131201300343810
36. Celardo, I., De Nicola, M., Mandoli, C., Pedersen, J.Z., Traversa, E., Ghibelli, L. (2011). Ce^{3+} ions determine redox-dependent anti-apoptotic effect of cerium oxide nanoparticles. *ACS Nano*, 5, 4537–4549. https://doi.org/10.1021/nn200126a
37. Maksimchuk, P.O., Hubenko, K.O., Seminko, V.V., et al. (2022) High antioxidant activity of gadolinium–yttrium orthovanadate nanoparticles in cell-free and biological milieu. *Nanotechnology*, 33, 055701. https://doi.org/10.1088/1361-6528/ac31e5
38. Foucquier, J., Guedj, M. (2015). Analysis of drug combinations: current methodological landscape. *Pharmacology Research & Perspectives*, 3, e00149. https://doi.org/10.1002/prp2.149
39. Korsvik, C., Patil, S., Seal, S., Self, W.T. (2007). Superoxide dismutase mimetic properties exhibited by vacancy engineered ceria nanoparticles. *Chemical Communications*, 10, 1056–1058. https://doi.org/10.1039/B615134E

40. Yun, J., Mullarky, E., Lu, C., et al. (2015). Vitamin C selectively kills KRAS and BRAF mutant colorectal cancer cells by targeting GAPDH. *Science*, 350, 1391–1396. https://doi.org/10.1126/science.aaa5004

Authors and Affiliations

Nataliya Kavok[1] · Galyna Dudetskaya[1] · Vladyslav Seminko[1,2]· Pavel Maksimchuk[1] · Yurii Kot[2] · Olga Sedyh[1] · Vladimir Klochkov[1] · Svitlana Yefimova[1]

Corresponding Author:
Vladyslav Seminko
seminko@ukr.net
https://orcid.org/0000-0002-3958-9161

[1] Institute for Scintillation Materials, National Academy of Sciences of Ukraine, 61072, 60 Nauky Ave., Kharkiv, Ukraine

[2] V. N. Karazin Kharkiv National University, 61022, 4 Svobody Sq., Kharkiv, Ukraine

Supplementary Files

This is a list of supplementary files associated with this preprint. Click to download.

- Supplement.docx